J. Fluid Mech. (1991), *vol.* 232, *pp.* 191–219
Printed in Great Britain

Stretching and breakup of droplets in chaotic flows

By M. TJAHJADI[1] AND J. M. OTTINO[2]

[1] Department of Chemical Engineering, University of Massachusetts, Amherst, MA 01003, USA
[2] Department of Chemical Engineering, Northwestern University, Evanston, IL 60208, USA

(Received 7 August 1990 and in revised form 19 April 1991)

We investigate the stretching and breakup of a drop freely suspended in a viscous fluid undergoing chaotic advection. Droplets stretch into filaments acted on by a complex flow history leading to exponential length increase, folding, and eventual breakup; following breakup, chaotic stirring disperses the fragments throughout the flow. These events are studied by experiments conducted in a time-periodic two-dimensional low-Reynolds-number chaotic flow. Studies are restricted to viscosity ratios p such that $0.01 < p < 2.8$.

The experimental results are highly reproducible and illustrate new qualitative aspects with respect to the case of stretching and breakup in linear flows. For example, breakup near folds is associated with a change of sign in stretching rate; this mode of breakup leads to the formation of rather large drops. The dominant breakup mechanism, however, is capillary wave instabilities in highly stretched filaments. Other modes of breakup, such as necking and end-pinching occur as well.

We find that drops in low-viscosity-ratio systems, $p < 1$, extend relatively little, $O(10^1–10^2)$, before they break, resulting in the formation of large droplets that may or may not break again; droplets in systems with $p > 1$, on the other hand, stretch substantially, $O(10^2–10^4)$, before they break, producing very small fragments that rarely break again. This results in a more non-uniform equilibrium drop size distribution than in the case of low-viscosity-ratio systems where there is a succession of breakup events. We find as well that the mean drop size decreases as the viscosity ratio increases.

The experimental results are interpreted in terms of a simple model assuming that moderately extended filaments behave passively; this is an excellent approximation especially for low-viscosity-ratio drops. The repetitive nature of stretching and folding, as well as of the breakup process itself, suggests self-similarity. We find that, indeed, upon scaling, the drop size distributions corresponding to different viscosity ratios can be collapsed into a master curve.

1. Introduction

The mechanical dispersion of immiscible fluids is of importance both in nature and in many industrial applications. Common industrial objectives involve dispersion of one fluid phase into another, either to form an emulsion, or to increase the interfacial area between the two phases for more efficient heat and/or mass transfer. Examples include blending of molten polymers to form two-phase structures of unique properties, dispersion of colour concentrates, mass transfer to bubbles in polymer devolatilization, and many more. The problem is of both practical and academic interest, and has thus received considerable attention in the fluid mechanics literature over the past fifty years starting with work by G. I. Taylor in 1934. As indicated by Taylor, some of the essential aspects of the problem can be captured by

studying the behaviour of a single droplet in linear flow and the central question is the determination of flow conditions which may result in drop breakup. There are two competing forces at work in drop deformation and breakup: the flow-induced stress tends to deform the drop and interfacial tension resists the deformation. Under some conditions, the interfacial forces are insufficient to balance the viscous stresses, and the drop elongates and breaks. The problem admits analytical and computational treatment but it is far from being completely understood. Most, if not all, of the analytical and computational work to date has been restricted to linear flows. Even in this relatively simple case, the equations of motion must be solved for the flow within and around the drop and boundary conditions applied on the surface of the drop, and the resulting drop shape must be determined as part of the solution. To date, no general solution has been found, but progress has been made through asymptotic analyses, considering conditions for which the drops are either spheroidal, or highly deformed. In addition, several numerical methods have been employed, but they have been limited to special flow conditions, e.g. axisymmetric extensional flow, plane hyperbolic flow, or shear flow, for particular values of the viscosity ratio (see review papers by Acrivos 1983 and Rallison 1984).

A relatively large number of experimental studies of drop behaviour in viscous shear flows have been reported; most works (Taylor 1934; Rumscheidt & Mason 1961; Grace 1971) consider drops in either two-dimensional irrotational flow or in simple shear flow. The analysis of intermediate flows, flow spanning the range between simple shear and pure extension, is relatively recent and requires a considerable increase in the sophistication of the experimental technique (Bentley & Leal 1986; Stone & Leal 1989*a*, *b*). However, in spite of the many experimental and theoretical works on drop deformation and breakup carried out in the past few decades, we are still unable to model breakup processes in realistic flows. Often the flow in systems of practical interest is complex and the velocity field that each drop experiences, as it moves through the flow, is not known. The deformation and breakup are related in a complicated way to the local velocity field and the fluid properties and, in general, they are affected by the presence of other drops. Clearly, simplifications are necessary in order to make the problem mathematically tractable.

This paper involves a combination of experimental and computational studies. The objective is to describe the deformation, fragmentation and dispersion of fluid drops freely suspended in a bulk fluid undergoing chaotic flow. The use of a chaotic flow is a means to an end; chaotic flows produce complex trajectories – mimicking those of more complex flows – but at the same time they admit careful experimentation and a fair degree of computation. However, the multiplicity of parameters and the richness of chaotic flows – involving regions of regularity and irregularity – makes a complete analysis rather forbidding and several simplifications are necessary. The experimental studies are restricted to very low volume fractions in such a way that in the companion theoretical analysis we can neglect hydrodynamic interactions between drops or fluid filaments. The flow conditions are restricted to global chaos in such a way that effects arising from regular regions (islands) can be negligible. As we shall see however, this still leaves several interesting physical phenomena; in fact, many modes of breakup, readily observed in chaotic flows, are difficult to observe or simply cannot happen in linear flows.

Flow visualization is the primary experimental tool and the study of mixing of passive tracers in the journal-bearing flow by Swanson & Ottino (1990) provides the starting point for the study conducted here. In fact, our investigation can be regarded as a study of the evolution of a dynamic structure – a highly stretched drop

or fluid filament – driven by a chaotic flow. In principle, we would like to find answers to the following kinds of questions: How do drops break in the chaotic and regular regions? What is the smallest drop size that can be produced with a given energy input? Is it possible to produce drops of an arbitrarily prescribed size? What is the nature of the drop size distribution; does it obey any kind of scaling behaviour? What aspects of the problem can be analysed computationally? How far can computations go? Obviously, this is a rather ambitious list and we will not be able to provide complete answers to all these questions. Nevertheless, we hope that the investigations reported here will help to clarify some of these questions and will provide a motivation for further study of the behaviour of droplets, and other microstructures, in chaotic flows.

The paper is organized as follows: §2 reviews some of the experimental and theoretical studies of drop breakup in linear flows with most of the attention focused on the case of 'infinitely' extended filaments; readers familiar with drop breakup may proceed directly to §3 which describes the apparatus, the kinematics of the flow, the fluids properties, and the visualization techniques. Section 4 is devoted to the presentation of experimental and computational results. Before we turn our attention to specific details it might be useful to discuss the nature of the comparisons between the experimental results and the computational predictions presented in §4. The comparison between figures is largely one-to-one. The bulk of the paper is built around a specific experiment, denoted as *experiment 1*, which is presented in figure 5. The rest of the presentation is devoted primarily to the interpretation of these results: figure 8 shows the patterns produced by the stretched and folded filament computed under the assumption that the filament is essentially passive; figures 9 and 11 show unravelled pictures of the filaments – figure 9 displays the characteristics of the flow field experienced by different parts of the filament whereas figure 11 shows the filament's radius along with the critical radius for breakup. The correspondence among these figures is one-to-one. Thus, figure 5(*d*), for example, can be compared directly with figures 8(*d*), 9(*d*), 11(*d*), and so on. It is expected that this correspondence will help the reader in getting a quick idea about the nature of the agreements and facilitate further comparisons between experiments and computations.

2. Drop breakup in linear flows

We consider a drop with initial radius r_d or a cylindrical filament with an initial radius a_0, with viscosity μ_i and density ρ_i, freely suspended in an infinite volume of a second fluid of viscosity μ_e and density ρ_e with interfacial tension σ (the subindices i and e represent the *interior* of the drop and the *exterior* fluid, respectively). In the neighbourhood of the drop or filament – but not near the interface – the velocity field with respect to a moving frame fixed on the centre of mass of the drop, denoted $\boldsymbol{X}$, is given by

$$\boldsymbol{v}^{\infty} = \boldsymbol{L}\cdot\boldsymbol{x} + \text{higher-order terms}, \tag{1}$$

where $\boldsymbol{L} = \boldsymbol{L}(\boldsymbol{X}, t) = (\nabla \boldsymbol{v})^{\mathrm{T}}$ is in general a function of time dictated by the macroscopic flow (we will refer to the flow expression (1) as a *microflow* associated with $\boldsymbol{X}$). Both fluids are assumed to be Newtonian and incompressible, and we assume as well that both the translation and rotation in the moving frame do not generate noticeable additional body forces and that the Reynolds number with respect to the droplet is small. Under these conditions the governing equations reduce to

$$\nabla P_m = \mu_m \nabla^2 \boldsymbol{v}_m, \quad \nabla\cdot\boldsymbol{v}_m = 0, \quad m = \mathrm{i}, \mathrm{e}, \tag{2}$$

and the appropriate boundary condition far from the drop is

$$\boldsymbol{v}_e \to \boldsymbol{v}^\infty = \boldsymbol{L}\cdot\boldsymbol{x} \quad \text{as} \quad |\boldsymbol{x}| \to \infty. \tag{3}$$

The velocity is continuous at the drop surface $S = S(\boldsymbol{x}, t)$,

$$\boldsymbol{v}_e = \boldsymbol{v}_i, \tag{4}$$

but the stress suffers a jump in the normal direction, $\boldsymbol{n}$, owing to the interfacial tension, σ,

$$(\boldsymbol{T}_e - \boldsymbol{T}_i)\cdot\boldsymbol{n} = \sigma\boldsymbol{n}\nabla\cdot\boldsymbol{n}. \tag{5}$$

The relevant parameters governing the behaviour of the system are the capillary number, $Ca_d = G\mu_e r_d/\sigma$ ($G = |\boldsymbol{D}|$, where $\boldsymbol{D} = \frac{1}{2}[\boldsymbol{L} + \boldsymbol{L}^T]$), which measures the relative importance of viscous and interfacial tension forces, the viscosity ratio, $p = \mu_i/\mu_e$, and the initial geometry of the drop.

The above equations contain no explicit time dependence. This implies that the velocity field at time t is determined by the drop shape and the instantaneous value of the imposed flow. In turn, the drop shape at time t is uniquely determined by the initial condition and the flow history, which in our case, is dictated by a (macroscopic) chaotic flow. The effect of the local flow on the deformation of a filament with orientation $\boldsymbol{m}$ can be quantified in terms of the mixing efficiency e_λ,

$$e_\lambda = (\boldsymbol{D}:\boldsymbol{mm})/\mathrm{G} = \alpha_\lambda/\mathrm{G}. \tag{6}$$

In general, e_λ varies erratically in chaotic regions and it is nearly time-periodic in regular regions (Ottino 1989). We shall have more to say about the behaviour of e_λ and G in §3.2.

In general, theoretical studies of drop deformation and breakup have been restricted to linear flows with constant $\boldsymbol{L}$ or to cases where $\boldsymbol{L}$ changes discontinuously (Stone & Leal 1989*b*). Studies can be divided into those dealing with drops with small deviation from sphericity (small-deformation analyses), and those dealing with highly elongated drops (large-deformation analyses). Since our study is closely related to capillary breakup of highly elongated drops (often referred to as fluid filaments or threads), we will focus entirely on the analyses of deformation and breakup of liquid threads.

Roughly speaking, a drop can be continuously stretched to form a 'long' liquid cylinder when its capillary number, Ca_d, exceeds its critical value, $Ca_{d,c}$ ($= G\mu_e r_d/\sigma$, the subscript d denotes 'drop'). Bentley & Leal (1986) have experimentally obtained the values of $Ca_{d,c}$ for a wide range of viscosity ratios ranging from pure-staining flow to simple shear flow. Once a drop is stretched to form a long thread, the breakup process is governed primarily by capillary waves. Most studies have been restricted to quiescent and axisymmetric extensional flow, and with some approximations, to shear and full three-dimensional linear flows. Thus, for example, within the confines of linear stability theory, the effects of viscosity ratio and disturbance wavelength on the disturbance growth rate and resulting drop size distribution are examined by Tomotika (1935), Rumscheidt & Mason (1962), and Lee & Flumerfelt (1981) for the case of quiescent fluids, by Tomotika (1936), Mikami, Cox & Mason (1975) for droplets in a shearing flow, and by Khakhar & Ottino (1987) for filaments in a linear three-dimensional flow. The results of these studies can be condensed in terms of a critical capillary number for the breakup of the filament, $Ca_{f,c}$ ($= G\mu_e a_c/\sigma$), where the subscript f denotes 'filament'.

A combination of these ideas provide a suitable starting point in the understanding of breakup in chaotic flows discussed in §4.2. For example, in order to study the

breakup of a stretched and folded filament, we follow subsegments, labelled by $\boldsymbol{X}$, as they are convected by a population of microflows, $\boldsymbol{L}(\boldsymbol{X}, t)$. For every location $\boldsymbol{X}$ there is a corresponding critical capillary number $Ca_{\mathrm{f,c}}$ such that instabilities in a subsegment with mean radius a_{m} and capillary number $Ca_{\mathrm{f}} (= G\mu_{\mathrm{e}} a_{\mathrm{m}}/\sigma)$ decay if $Ca_{\mathrm{f}} > Ca_{\mathrm{f,c}}$, or grow if $Ca_{\mathrm{f}} < Ca_{\mathrm{f,c}}$ (equivalently the ideas can be phrased in terms of the mean radius a_{m} and the critical radius a_{c}, i.e. if the radius is *below* some critical value a_{c} the amplitude grows).

Let us consider the implementation of these ideas in more detail. Assume an infinitely extended filament of radius a in a microflow $\boldsymbol{L}\cdot\boldsymbol{x}$. The radius of the filament is given by

$$a = a_{\mathrm{m}} + \epsilon f(z), \tag{7}$$

where z is a coordinate along the filament, and $\epsilon f(z)$ is a small varicosity due to small disturbances (it can be argued that the asymmetric variation due to shear is small (Khakhar & Ottino 1987) and accordingly we neglect such effects to simplify the analysis). Typically $f(z)$ is assumed to have a sinusoidal form (Tomotika 1935)

$$f(z) = A\cos(kz), \tag{8}$$

where A is the amplitude, $k = 2\pi/\Lambda$ the wavenumber, and Λ the wavelength. An analysis based on Mikami *et al.* (1975) and Khakhar & Ottino (1987) gives that the dimensionless wavenumber, $x = ka_{\mathrm{m}}$, as

$$\dot{x} = -\tfrac{3}{2} e_\lambda x \tag{9}$$

and the amplitude as

$$\dot{A} = \tfrac{1}{2}A\left\{-e_\lambda + \frac{1}{Ca_{\mathrm{f}}}\left(\frac{x_0}{x}\right)^{\frac{1}{3}}(1-x^2)\,\phi(x,p) - 3e_\lambda(p-1)\,\phi'(x,p)\right\}, \tag{10}$$

where $Ca_{\mathrm{f}} = G\mu_{\mathrm{e}} a_{\mathrm{m}}/\sigma$, x_0 is the initial wavenumber, and $\phi(x,p)$ and $\phi'(x,p)$ are rather complicated functions of the wavenumber and viscosity ratio. Notice that stretching rate e_λ enters as an input in all equations. In our case α_λ or e_λ are typically complex functions of time. However, in order to simplify matters, we will assume that e_λ is constant (> 0).

A convenient way of looking at the evolution of disturbances in the filament is in terms of the magnification M which is defined such that

$$M = \begin{cases} \ln(A/A_\epsilon) & \text{for } x < x_{\mathrm{c}}, \quad A > A_\epsilon \\ 0 & \text{for } x > x_{\mathrm{c}}, \end{cases} \tag{11}$$

where A_ϵ is the amplitude of disturbances due to thermal fluctuations and x_{c} is the critical wavenumber (i.e. the wavenumber such that disturbances are changing from decaying to growing). Following Kuhn (1953), the value of A_ϵ is obtained as $A_\epsilon = [21kT/(8\pi^{\frac{3}{2}}\sigma)]^{\frac{1}{2}}$, where k is Boltzmann's constant, and T the absolute temperature (this yields values of A_ϵ in the range 10^{-7}–10^{-8} cm; other authors (Rumscheidt & Mason 1962) use higher values in the range 10^{-5}–10^{-6} cm). The dynamics of the growth of disturbances leading to the breakup of the thread may be visualized in terms of figure 1, in which both the mean radius of the filament, a_{m}, and the magnification of the disturbances, M, are plotted for various x_0 as a function of time. There is only one optimum wavenumber, denoted $x_{0,\mathrm{opt}}$, that corresponds to the maximum rate of growth. According to this picture breakup occurs when the mean radius, which decreases with time due to stretching, equals the amplitude of disturbance A corresponding to $x_{0,\mathrm{opt}}$ (i.e. when M crosses with $\ln(a_{\mathrm{m}}/A_\epsilon)$).

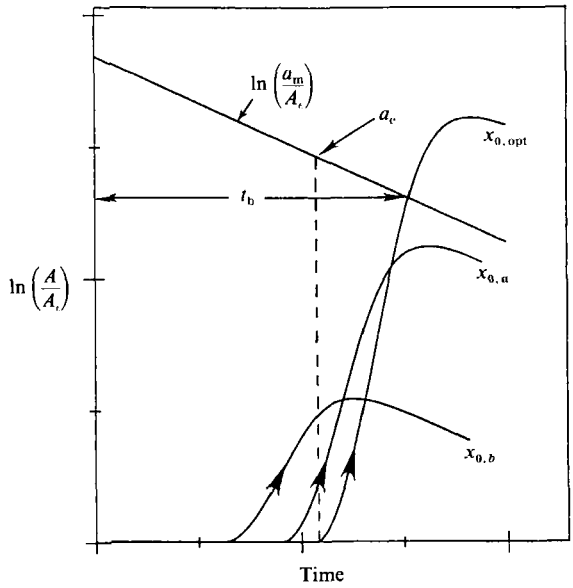

FIGURE 1. Magnification of disturbances, A/A_ϵ, in a linear flow for a fixed value of shear rate G, stretching rate e_λ, viscosity ratio p, and different initial wavenumbers. The straight line is the dimensionless mean radius, a_m/A_ϵ, versus time for the same conditions. The intersection of the magnification corresponding to the optimum dimensionless wavenumber, $x_{0,\mathrm{opt}}$, and the straight line gives the point of breakup. Note the definition for the time of breakup t_b, the critical radius a_c.

It is illustrative to indicate how to obtain the optimum wavenumber, $x_{0,\mathrm{opt}}$, and the critical wavenumber x_c. The computational steps are as follows:

(i) input the parameters $p, e_\lambda, Ca_f, a_m/A_\epsilon$; select a tolerance ϵ;

(ii) guess or input $(x_0)_i (> 1)$, and compute M and $\ln(a_m/A_\epsilon)$;

(iii) check if M crosses with $\ln(a_m/A_\epsilon)$; if yes, record the time required for breakup, t_b, if not, increase x_0 and return to step (ii);

(iv) calculate M at t_b for a range of x_0, and pick the new x_0, $(x_0)_{i+1}$, that corresponds to the largest M; if $(x_0)_{i+1} - (x_0)_i > \epsilon$ then return to step (ii), if $(x_0)_{i+1} - (x_0)_i < \epsilon$ then $x_{0,\mathrm{opt}} = (x_0)_{i+1}$.

The solution $x_{0,\mathrm{opt}}$ corresponds to the shortest breakup time; therefore the disturbance with wavenumber $x_{0,\mathrm{opt}}$ is magnified the fastest. On the other hand, the critical wavenumber x_c is obtained by means of the following conditions:

$$\left(\frac{\partial \ln A}{\partial \ln x}\right)_{x=x_c,\, x_0=x_{0,\mathrm{opt}}} = 0 \tag{12}$$

and

$$\left(\frac{\partial^2 \ln A}{\partial \ln x^2}\right)_{x=x_c,\, x_0=x_{0,\mathrm{opt}}} > 0. \tag{13}$$

Finally, the critical radius of the filament, a_c, is related to the critical wavenumber, x_c, by

$$a_c = a_m (x_c/x_{0,\mathrm{opt}})^{\frac{1}{3}}, \tag{14}$$

where a_m is the value we input in step (i) above. We are now in a position to compute $Ca_{f,c}$ and a_c. Curve-fitting of computational results gives that

$$a_c(\mathrm{cm}) = (37.8 \pm 3.8) 10^{-4} e_\lambda^{-0.89} p^{-0.44} (\sigma/\mu_e G)^{\chi}, \tag{15}$$

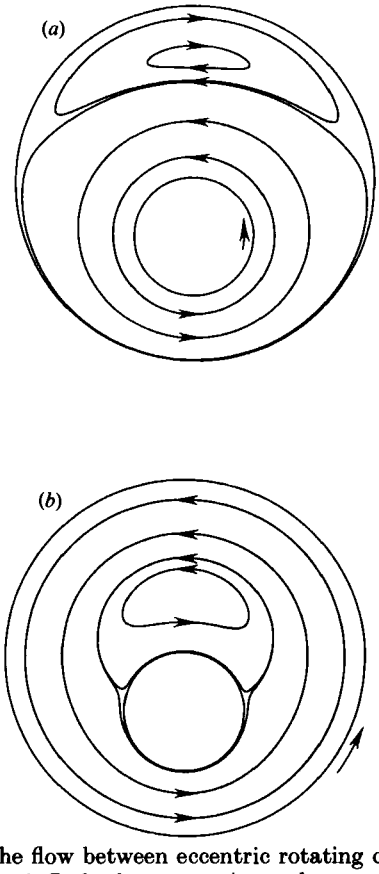

FIGURE 2. Streamlines in the flow between eccentric rotating cylinders. (*a*) $v_{in} > 0$, $v_{out} = 0$. (*b*) $v_{in} = 0$, $v_{out} > 0$. In both cases $r_{in}/r_{out} = \frac{1}{3}$, eccentricity/$r_{out} = 0.3$.

where $0.84 < \chi < 0.92$ for $10^{-3} < p < 10^2$; $(\mu_e G/\sigma)$ is in cm^{-1} and A_ϵ is taken to be 10^{-7} cm. Equation (15) indicates that the critical capillary number for the filament, $Ca_{f,c}$ $(= G\mu_e a_c/\sigma)$ is typically much less than one and less than $Ca_{d,c}$. Note that (15) is obtained assuming e_λ is constant and positive. Given the nature of the assumptions, comparisons between a_m and a_c are restricted to regions where $e_\lambda > 0$, and are warranted provided that the timescale of variations in the imposed flow field, de_λ/dt, is slower than the timescale of the fastest growing capillary waves, dA/dt.

3. Flow system, kinematics, and experimental techniques

3.1. *Journal-bearing flow: apparatus and fluids*

The journal bearing consists of two eccentric rotating cylinders moving in the same or opposite directions with constant or time-varying angular speeds v_{in} and v_{out}. At low Reynolds and Strouhal numbers the flow is two-dimensional and the instantaneous stream-function portrait depends only on the geometry and the ratio v_{in}/v_{out}. A large variety of two-dimensional flows can be generated depending on (i) the ratio of the radii of the inner cylinder to the outer cylinder, (ii) the distance of the centre of the inner cylinder from the centre of the outer cylinder (eccentricity), and (iii) the ratio of velocities of the inner and outer cylinders. Several alternative

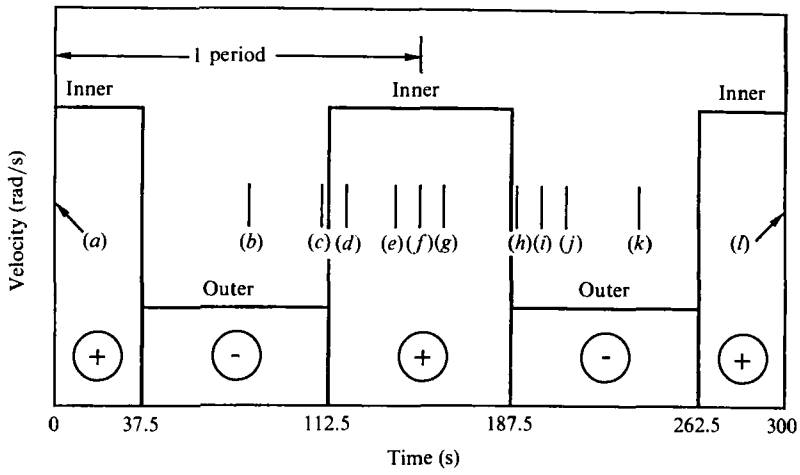

FIGURE 3. Discontinuous velocity protocol corresponding to experiment 1 in §4.1. The designation (*a*), (*b*),..., etc. corresponds to the photographs in figures 5 and 8.

versions of analytical solutions for the stream function are available; here we use the one due to Wannier (1950) which has the advantage of being given in (x, y)-coordinates. Streamlines of steady flows with only one wall in motion are shown in figure 2. If the flow is made time periodic, the flow pattern changes with time so that the streamlines at time t cross the streamlines at time $t+\Delta t$ and, therefore, chaos is likely (Ottino 1989). In particular, the system produces chaos when both cylinders are forced in a time-periodic manner (both v_{in} and v_{out} have identical period T in everything that follows). The various types of forcing motions, $v_{\text{in}}(t)$ and $v_{\text{out}}(t)$, are quantified in terms of the rotation of the inner or outer cylinder per period,

$$\theta_{\text{in}} = \frac{1}{2\pi}\int_0^T v_{\text{in}}(t)\,\mathrm{d}t, \quad \theta_{\text{out}} = \frac{1}{2\pi}\int_0^T v_{\text{out}}(t)\,\mathrm{d}t. \tag{16a, b}$$

For simplicity, the ratio of θ_{in} and θ_{out} will be kept constant, and a discontinuous velocity protocol, where only one cylinder is in motion at any particular instant of time, will be used (see figure 3: the locations denoted (*a*), (*b*),..., (*l*) correspond to the snapshots taken in figures 5 and 8).

Chaos in the journal-bearing flow was first experimentally and computationally studied by Chaiken *et al.* (1986) and further computational studies are reported by Aref & Balachandar (1986). The emphasis in both of these works was on demonstrating that chaos was indeed possible in a physically realizable low-Reynolds-number flow. More recently, Swanson & Ottino (1990) used this flow to compare several computational and experimental techniques to predict the mixing of passive tracers when the mixing is widespread and occurs in only a few number of periods. It should be noted that in the case of mixing of passive tracers in creeping flows, the actual wave form of the cylinder velocities is not important, and as long as $v_{\text{in}} = 0$ when $v_{\text{out}} \neq 0$ and vice versa, only their displacements θ_{in} and θ_{out} affect the results (Swanson & Ottino 1990). However, if the fluids are immiscible, time enters explicitly in the evolution of the drop filament and the exact form of both $v_{\text{in}}(t)$ and $v_{\text{out}}(t)$ becomes important.

The experimental apparatus is the same as the one used by Swanson & Ottino (1990). The bottom of the outer cylinder is transparent so that pictures of the whole flow area can be obtained from below. The speed of the motors is monitored by a

(*a*)

	Fluids	μ(c.p.s.)[a]	ρ(g/cc)	μ(P)[b]
A	No. 40 oil	110000	1.02	
B	1-Bromonaphthalene	$O(10^1)$	1.49	
	Corn syrup 1632	32600	1.42	$2.87 \times 10^7\, T^{-3.63}$
	Fomblin® YL Vac 06/6	120	1.88	
	Mineral oil	35	0.88	

(*b*)

Drop fluid no.	μ_i(c.p.s.)[a]	$p(\mu_i/\mu_e)$[a]	σ(dyne/cm)	μ(P)[b]
1 (0.90A+0.10B)[c]	91000	2.8	9.1	$4.64 \times 10^5\, T^{-1.99}$
2 (0.67A+0.33B)	13200	0.40	9.5	$2.12 \times 10^5\, T^{-2.35}$
3 (0.50A+0.50B)	2100	0.064	10.0	$2.36 \times 10^4\, T^{-2.22}$
4 (0.33A+0.67B)	330	0.010	10.4	$1.18 \times 10^2\, T^{-1.14}$

[a] $T = 23$ °C.
[b] The equations are valid for 20 °C $\leqslant T \leqslant$ 30 °C, T is in °C.
[c] Volume fraction.

TABLE 1. (*a*) Fluid properties; (*b*) properties of fluid systems used

computer and the angular displacements are controlled to 99% accuracy. The radius of the outer cylinder, r_{out}, is 7.62 cm and the inner cylinder, r_{in}, is 2.54 cm. The eccentricity is 2.29 cm.

The magnitude of inertial terms is given by the Reynolds number, $Re = \rho_e v(r_{out}-r_{in})/\mu_e$, and Strouhal number of the apparatus, $St = (r_{out}-r_{in})/vT$, where $v = \max(r_{in}v_{in}, r_{out}v_{out})$ and T is a period of oscillation for the velocities. The Reynolds number corresponding to a drop of size r_d is given by $Re_d = \rho_i Gr_d^2/\mu_i$. In a typical experiment, Re is about 10^{-2}, St is about 10^{-1}, and Re_d is about 10^{-7} to 10^{-4}.

The suspending fluid used in the experiments is corn syrup 1632 (Corn Products of Englewood Cliffs, NJ). The drop fluid is a mixture of no. 40 oil, an oxidized castor oil available from CasChem Inc. of Bayonne, NJ, and 1-Bromonaphthalene (Aldrich Chemical). These fluids have been reported to be Newtonian (Bentley & Leal 1986; Rumscheidt & Mason 1961).

The procedure to make the fluids for the drops is as follows. First, organic dye (Oil Blue N, or Oil Red O, Aldrich Chemical) is dissolved in 1-Bromonaphthalene. Then some specific amount of 1-Bromonaphthalene is mixed with oil no. 40 until the mixture becomes homogeneous (several days). Depending on the volume fraction of 1-Bromonaphthalene, the viscosity of the mixture can be varied from 10^1 to 10^4 cP. Buoyancy effects due to density difference between the bulk and the immersed fluid cannot be completely eliminated; they are however relatively unimportant, especially when the drops are small ($r_d < 0.5$ mm). During the course of an experiment (approximately 20 min), large liquid drops (approximately 1 mm in diameter) might rise about 0.5 cm in the vertical direction. Bottom effects are minimized by floating the working fluid on a denser and less viscous fluid (perfluoropolyether vacuum-pump oil; Fomblin® YL Vac 06/6, Aldrich). This bottom fluid is more convenient than the fluid used in the previous experiments (Swanson & Ottino (1990) used 1-Iodo-3-methylbutane); it is much denser, transparent, non-volatile, and about 85% recoverable when cleanup of the apparatus is called for. A thin layer of mineral oil is poured on top of the corn syrup to inhibit crystallization. Table 1 (*a*) shows the properties of the fluids used. The viscosities of the fluids are measured using a shear-stress rheometer (Rheometrics) and a rotary

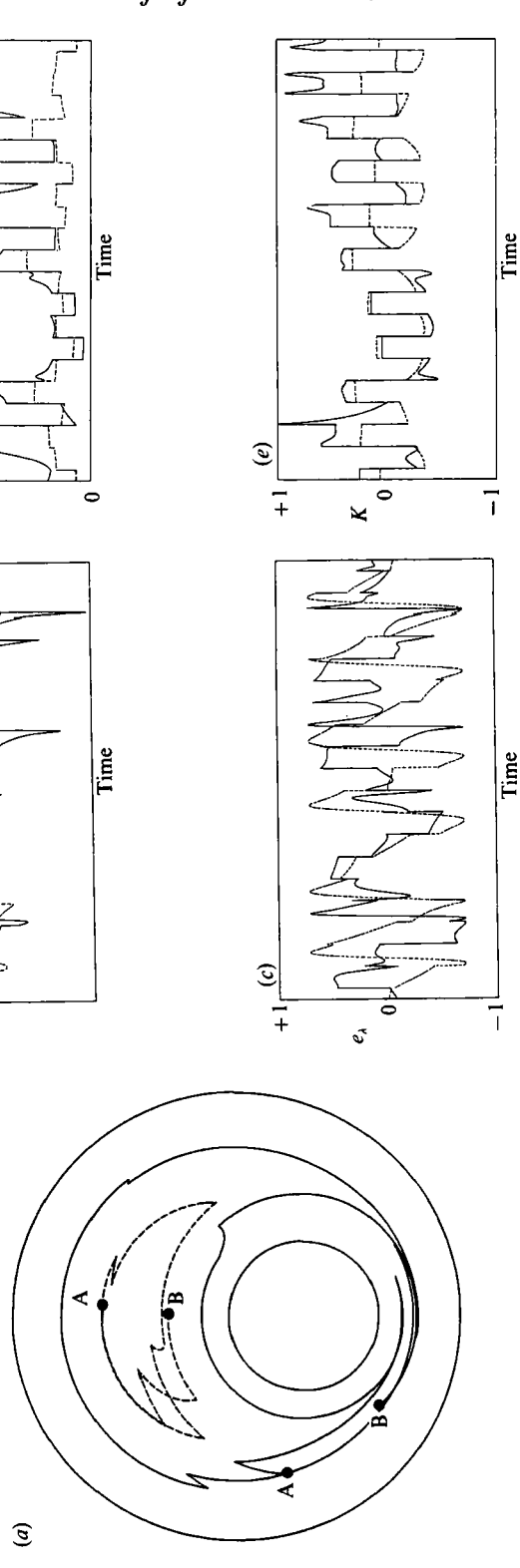

FIGURE 4. Typical behaviour of kinematics in regular and chaotic regions. (*a*) Pathlines of two fluid particles placed in a chaotic region (solid line) and in a regular region (dashed line). The initial position is denoted A, the final position is denoted B. (*b–e*) Behaviour of α_λ, e_λ, G, and K respectively as a function of time (chaotic region, solid line; regular region, dashed line).

viscometer (Cole Palmer). The interfacial tension of the drop fluids is estimated from the drop deformation experiments in a Couette flow using linear theory (Taylor 1934). Table 1 (*b*) shows the values of viscosities as a function of temperature for the drop fluids used.

3.2. *Kinematics in regular and chaotic regions*

The character of the velocity field in the neighbourhood of a moving particle, which acts as forcing to the evolution equations for the filament (equations (9) and (10)), can be characterized in terms the stretching rate, α_λ, and the efficiency e_λ, which are defined as follows (Ottino 1989). The rate of change of a material filament $\mathrm{d}\boldsymbol{x}$ with initial length $\mathrm{d}\boldsymbol{X}$ is given by

$$\dot{\overline{\mathrm{d}\boldsymbol{x}}} = \mathrm{d}\boldsymbol{x}\cdot\nabla\boldsymbol{v}, \tag{17}$$

and the rate of change of length stretch, $\lambda\,(\equiv|\mathrm{d}\boldsymbol{x}|/|\mathrm{d}\boldsymbol{X}|)$ is given by

$$\dot{\lambda}/\lambda = \boldsymbol{D}:\boldsymbol{mm}, \tag{18}$$

where $\boldsymbol{m} = \mathrm{d}\boldsymbol{x}/|\mathrm{d}\boldsymbol{x}|$ and the overdot represents the material time derivative. The Lagrangian history $\dot{\lambda}/\lambda = \alpha_\lambda(\boldsymbol{X},\boldsymbol{M},t)$ is called the *stretching function*, and is in general a function of initial orientation, $\boldsymbol{M} = \mathrm{d}\boldsymbol{X}/|\mathrm{d}\boldsymbol{X}|$, and initial location, $\boldsymbol{X}$. The stretching efficiency, $e_\lambda = e_\lambda(\boldsymbol{X},\boldsymbol{M},t)$ is defined as

$$e_\lambda \equiv (\dot{\lambda}/\lambda)/(\boldsymbol{D}:\boldsymbol{D})^{\frac{1}{2}} = \alpha_\lambda/G < 1. \tag{19}$$

The efficiency e_λ is constant in hyperbolic flows, and has a maximum value of $1/\sqrt{2}$ in two-dimensional flows and $(2/3)^{\frac{1}{2}}$ in three-dimensional flows. On the other hand, the efficiency in shear flows, and in fact in all steady bounded two-dimensional flows, decays as $1/t$ (Ottino 1989). Of more interest to us is the behaviour of α_λ and e_λ in chaotic flows. There are two clearly distinguishable types of behaviour: within chaotic regions α_λ and e_λ vary erratically, have nearly constant long-time average, and the length stretch is exponential in time. On the other hand, within regular regions, α_λ and e_λ vary in a nearly time-periodic manner and the length stretch is linear in time.

Another way to make evident the shear-like *vs.* elongational-like character of the local two-dimensional flow, is in terms of $K = |\boldsymbol{D}-\boldsymbol{\Omega}|/|\boldsymbol{D}+\boldsymbol{\Omega}|$, where $\boldsymbol{\Omega} = \frac{1}{2}[\boldsymbol{L}-\boldsymbol{L}^{\mathrm{T}}]$. The parameter K is indifferent, i.e. it does not depend on the frame used, and ranges from $K = +1$ for orthogonal stagnation flow to $K = -1$ for pure rotational flow ($K = 0$ corresponds to simple shear flow). In general the connection between α_λ, e_λ, G, and K is rather complicated and only a few points will be highlighted here.

Figure 4 (*a–e*) illustrates typical flow histories, α_λ, e_λ, G, and K, in the neighbourhood of two fluid particles placed in regular and chaotic regions of the flow. The behaviour of α_λ and e_λ depends on the initial orientation; on the other hand the histories of G and K depend only on the instantaneous placement in the flow. It is apparent that a fluid filament placed in a regular region experiences a nearly periodic history of stretching and compression, alternating positive and negative values of α_λ, whereas a fluid filament in chaotic regions experiences a complicated time history with a positive time average. Note also that the rate of stretching in chaotic regions quickly becomes independent of initial conditions. Similar conclusions can be drawn from the behaviour of e_λ. In general, there is a wide distribution of stretching histories within the chaotic regions of the flow. However, most of these effects become evident only after a large number of periods and for the purposes of our discussion they will not be considered here.

3.3. *Photography and digital image analysis*

All photography is taken using a 35 mm camera (Nikon F3) with a micro lens (Nikkor 200 mm) with 4× magnification. A scale is placed in the fluids for a more precise size measurement. The types of films vary (Kodak Tmax or Ektachrome) depending on the objective of the experiment. We use Kodak F/M paper to make B/W prints or Ilford Cibachrome paper to make colour prints. The size of an object in the final print can be enlarged up to 50× its original size without apparent loss of resolution.

Photographs of the droplets are digitized and the drop size is measured using the Image-Pro Software from Media Cybernetics, Inc. Enlarged photographs from each set of experiments are cut into small pieces ($O(100)$). Each of these small photographs, which has about 10–50 drops, is grabbed by the digital camera and projected to a 512×480 pixel TV screen. This procedure is carried out to ensure that the smallest drops are still represented by a minimum of $O(10)$ pixels. Small droplets present some problems due to contrast (primarily due to the small amount of dye contained in the drops and three-dimensionality). To overcome this problem we define some threshold value for the intensity (i.e. between 0 and 255 for B/W); if a pixel has a value above or below the threshold it is made completely white or black, respectively. In experiments where we need to measure the size of very small droplets, satellites, and sub-satellites, or to capture the dynamics of the satellites formation, we resort to a stereomicroscope with magnification up to 63×. This procedure is used to obtain the results presented in figure 7.

4. Results

4.1. *Drop breakup in a chaotic flow: a typical case*

Experiment 1 corresponds to a discontinuous counter-rotating velocity protocol, shown in figure 3, with $v_{in} = (r_{out}/r_{in})\, v_{out} = 0.50$ rad/s; these conditions correspond to a globally chaotic flow. The drop placed in the bulk fluid corresponds to the fluid no. 3 shown in table 1 (*b*). Since the results that follow here are representative of a large number of repeated experiments, a comment about the reproducibility of results seems in order. To the extent that it is impossible to place a droplet in exactly the same location twice, and because chaos magnifies the effect of errors in the initial conditions, it is rather hopeless to expect that two experiments will produce exactly the same number of drops, especially when the experiment generates thousands of drops, or that the thousands of droplets will be located in precisely the same spatial locations. All these features are small-scale details. Large-scale features, however, are highly reproducible. Large-scale features are, for example, the spatial distribution of the filament, the location and times where breakup occurs, the placement and nesting of folds and the mode of breakup associated with them, as well as information of a more average character, such as the final drop size distribution generated after the breakup.

The dynamics of elongation and breakup of a drop placed in the flow are shown in a series of pictures in figure 5(*a–l*) (plate 1). Initially, a drop with a radius approximately 0.4–0.5 cm, is injected about 5 cm below the surface of the bulk fluid by means of a syringe/pipet (figure 5*a*, $t = 0$ s). First, the inner wall moves clockwise for 6π rad ($\theta_{in} = 12\pi$ rad) and the drop is translated and stretched by the flow. Then the inner wall stops, the outer wall starts moving counterclockwise ($\theta_{out} = 4\pi$ rad). The drop, which has extended into a 'fat fluid filament', continues to be elongated

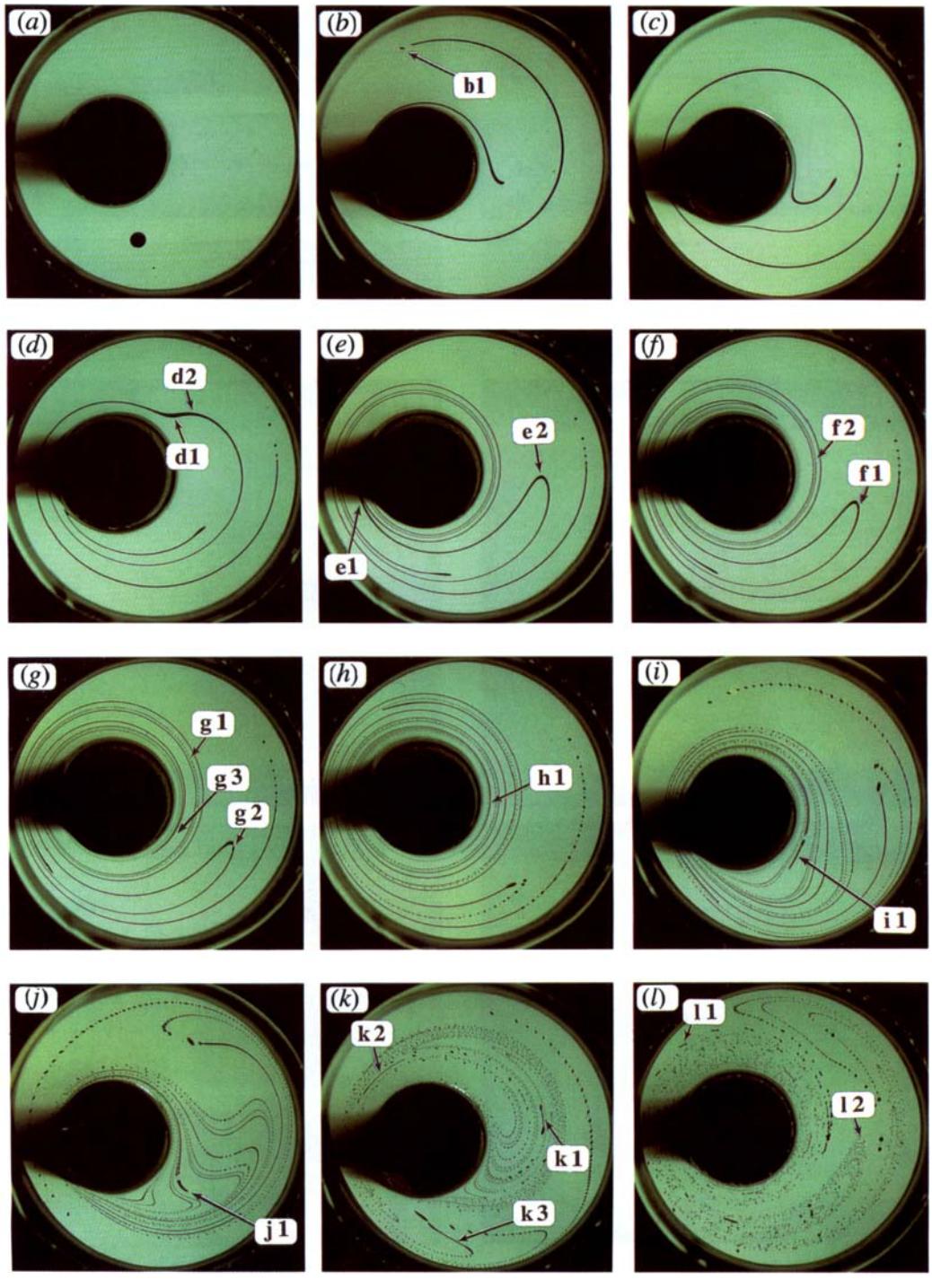

FIGURE 5. Dynamics of elongation, folding, and breakup of a drop placed in a globally chaotic flow (experiment 1). The viscosity ratio p is 0.067. The times corresponding to photographs (a–l) are shown in figure 3.

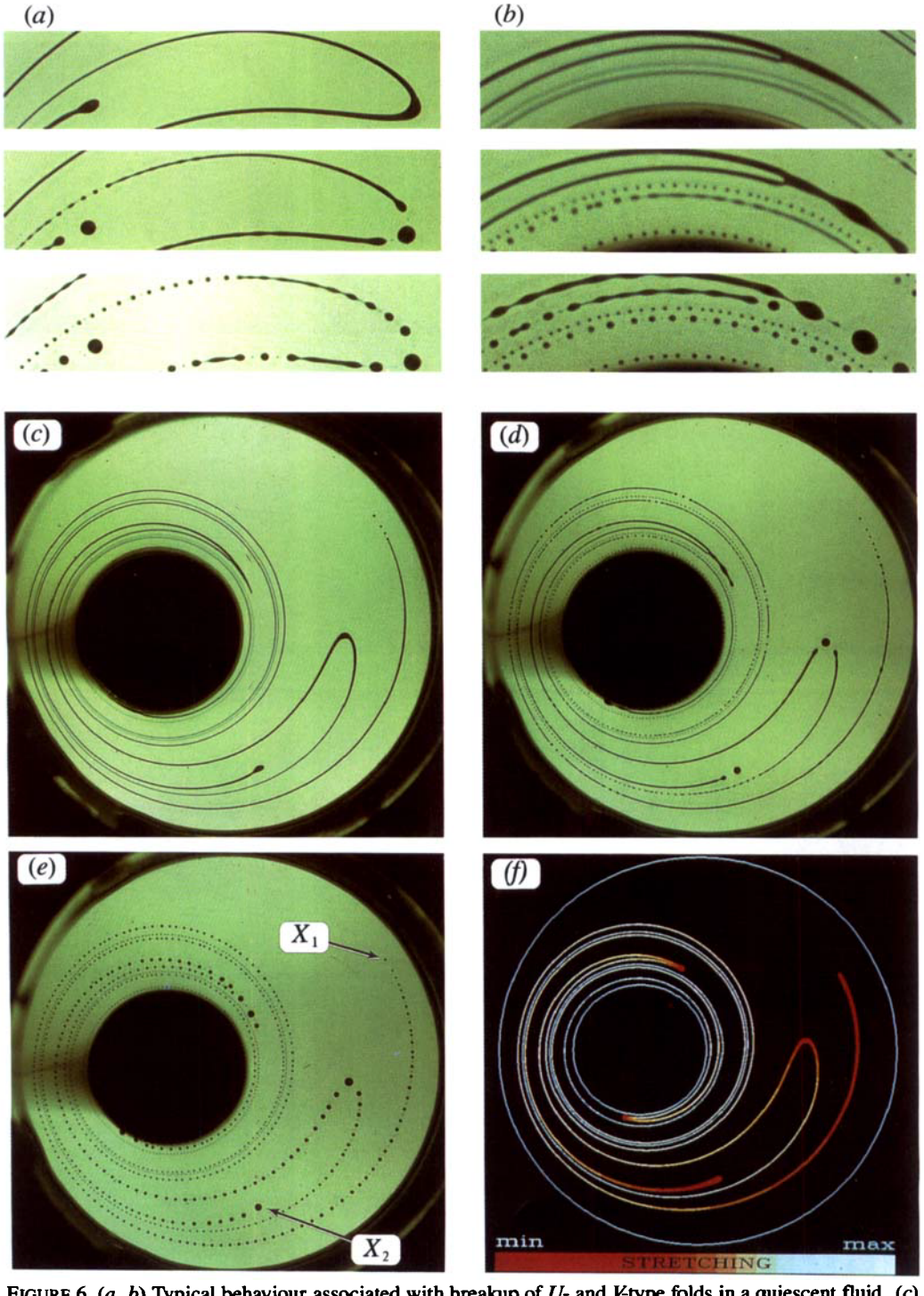

FIGURE 6. (*a*, *b*) Typical behaviour associated with breakup of *U*- and *V*-type folds in a quiescent fluid. (*c*) Elongation and folding of a drop ($p = 0.40$) at the end of period 1; then the flow is stopped. (*d*) Breakup processes along the filament 20 s after the flow is stopped. (*e*) The drop fragments after the breakup is complete. The corresponding computer-generated picture of the unbroken fluid filament is shown in (*f*). The colour scale corresponds to the amount of length stretch: white indicates maximum, red minimum.

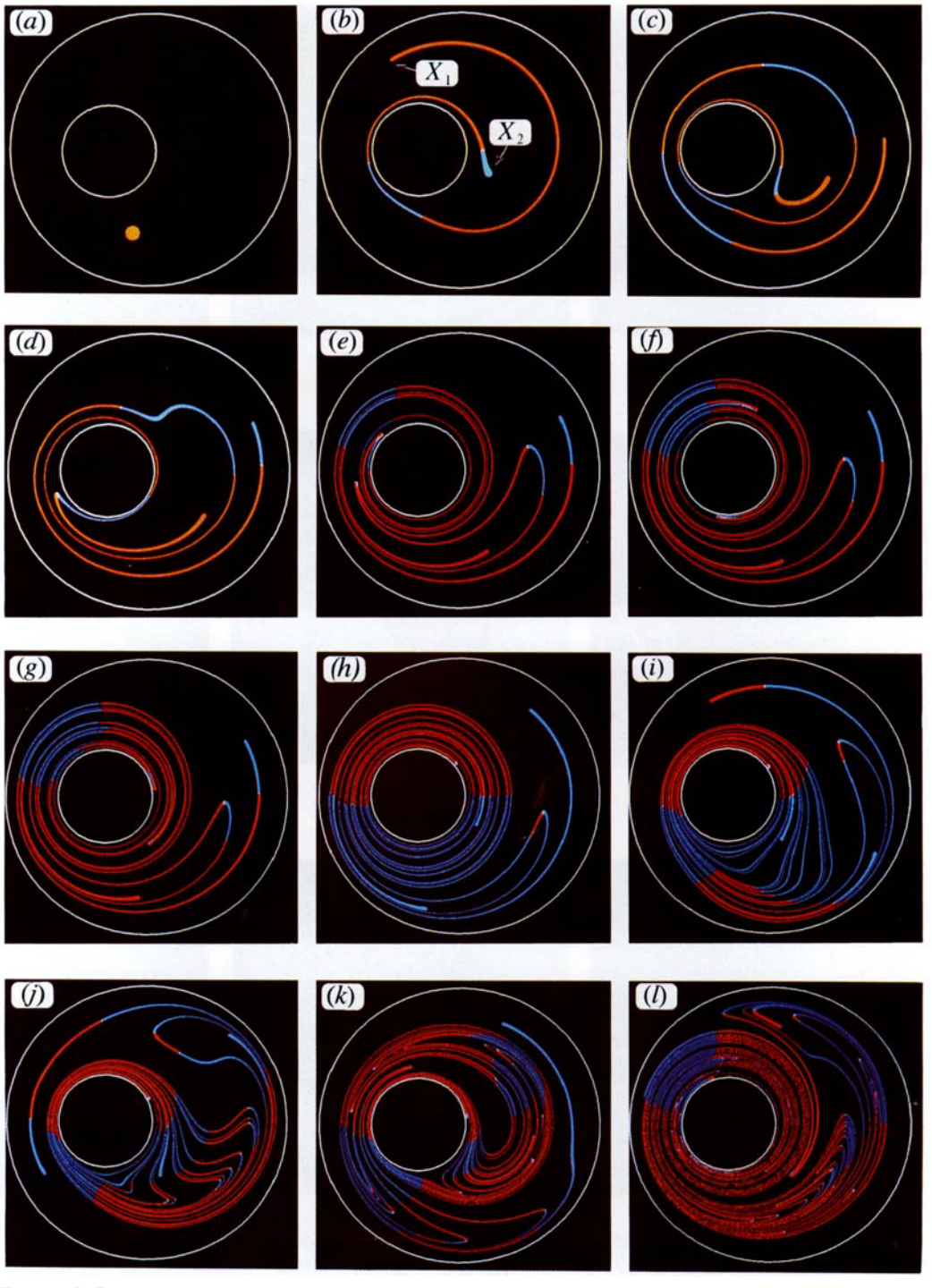

FIGURE 8. Patterns produced by the stretched and folded filaments corresponding to experiment 1. Two colours are used to differentiate the stretching sign: red corresponds to positive stretching ($e_1>0$), blue to negative stretching ($e_1<0$). The beginning and end of the filament are denoted X_1 and X_2, shown only in (*b*); the same notation is used in figures 9 and 11.

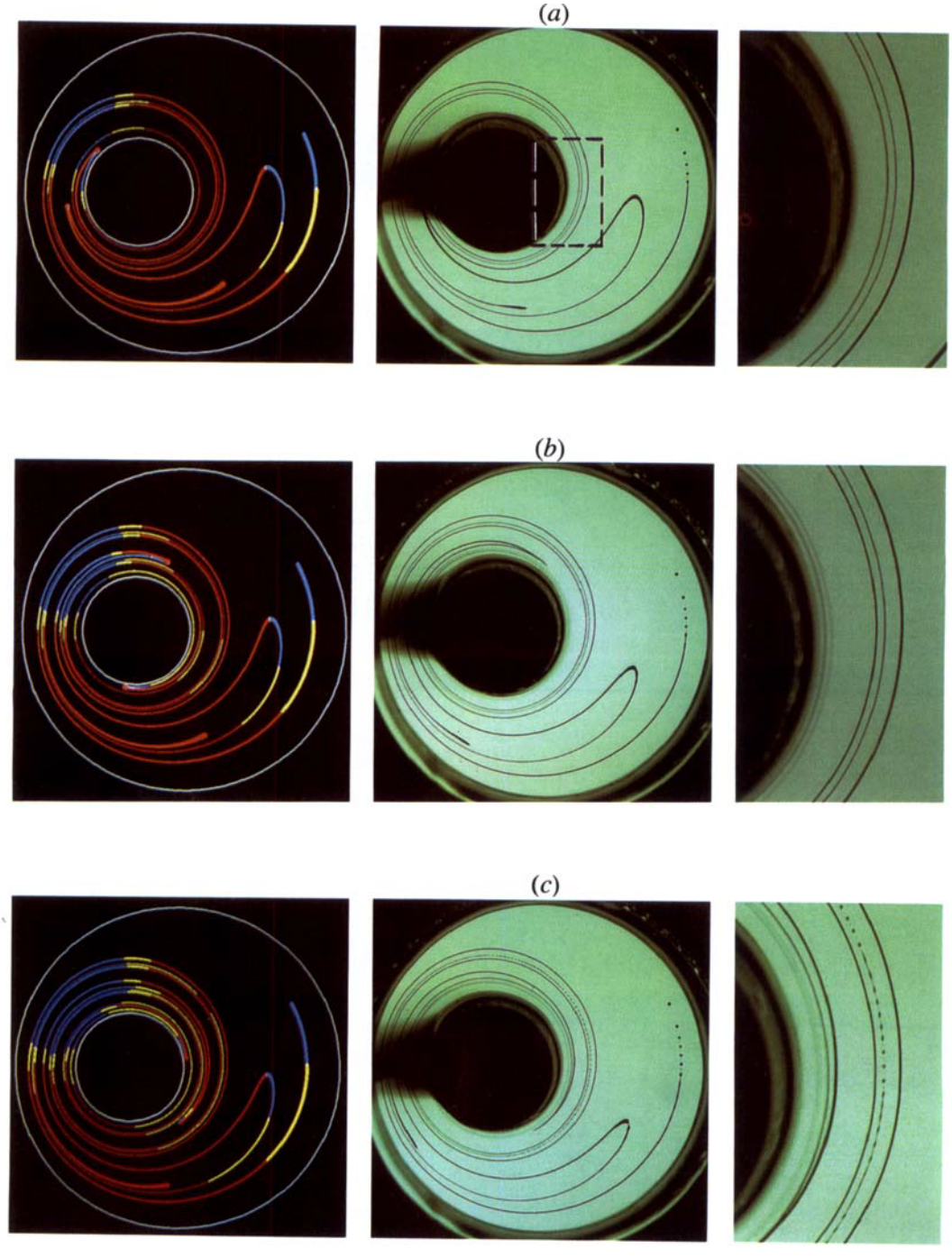

FIGURE 12. Comparison of the locations of breakup obtained in the experiments versus computations: (*a*) corresponds to figure 5(*e*), (*b*) to 5(*f*), and (*c*) to 5(*g*). The computational results are shown in the left column. Two colours are used to differentiate the stretching sign: red corresponds to positive stretching ($e_\lambda > 0$), blue to negative stretching ($e_\lambda < 0$). Yellow corresponds to the region where $a_m < a_c$, and $e_\lambda > 0$. The figures in the right column show a magnified view of the development of the instabilities, the approximate location of which is shown by the dashed box in the top middle column.

and breakup occurs at one end of the filament by means of a mechanism similar to end-pinching (arrow b1, figure 5*b*, $t = 80$ s); however, the number of droplets produced by this mode of breakup is rather insignificant. Once the initial drop has been stretched by a factor of 20 or so, the rate of deformation approaches that of a passive material line and the rate of length generation is exponential (please, see figure 10).

When the outer cylinder stops and the inner wall moves in the clockwise direction (figure 5*d*, $t = 120$ s), the filament gives birth to two new folds identified by arrows d1 and d2. The swelling around the folds suggests that the filament is being compressed by the flow. The folds evolve into two qualitatively different types: a pointed V-shape fold (e1), and a rounded U-shape fold (e2) shown in figure 5(*e*) ($t = 140$ s). There is a noticeable development of capillary instability slightly to the right of the tip of the U-shape fold and at the end of one period, $t = 150$ s (figure 5*f*), the capillary instabilities near the U-shape fold have grown larger and breakup is about to occur (arrow f1).

During the flow, disturbances along the surface of the stretched filaments, away from folds and ends, are damped in spite of the small radius of the filaments. However, given enough time (under flow), the radii of the threads decrease further and when interfacial tension becomes important, disturbances magnify. These disturbances are not yet present in figure 5(*b–e*) but a magnified view of figure 5(*f*) shows unmistakable signs of capillary instabilities (arrow f2). Subsequently breakup occurs along the stretched filament (arrow g1 in figure 5*g*, $t = 160$ s) as well as near the U-fold (arrow g2). Shortly thereafter capillary wave instabilities appear in various regions of the filaments and fragmentation occurs rather rapidly afterwards (figure 5*h*, $t = 190$ s).

The majority of breakups are caused by the growth of capillary disturbances on the surface of extending fluid filaments and this mechanism gives rise to the formation of droplets of widely different sizes. Between two large drops there is a satellite drop (see figure 5*h*); in the neighbourhood of the satellite drop, there are sub-satellites, and between sub-satellites, sub-sub-satellites, and so on. The ratio of radii between the mother drops and the smallest satellite, observed under a stereoscope, can be as high as three orders of magnitude (some pictures of satellites, sub-satellites, and so on, appear in Tjahjadi & Ottino 1990).

On the other hand, some of the largest drop fragments are a consequence of folds. Figure 6(*a*, *b*) (plate 2) shows a magnified view of the typical breakup processes associated with U- and V-type folds. Often folds produce even bigger fragments. Consider for example the evolution of the tip of the V-shape fold in figure 5(*e*) (arrow e1) as it extends into a slender filament (arrow g3, figure 5*g*, $t = 160$ s). When the inner wall stops and the outer wall starts moving the fold is compressed and pinches off at the juncture where the two upper branches meet the one lower branch (arrow h1, figure 5*h*, $t = 190$ s). The separated lower branch of the Y-fold – a slender drop about 2 cm long – and its neighbouring fluid filaments are folded by the 'new' flow. Figure 5(*i–k*) shows the slender drop being compressed (arrows i1, j1) to about one-third of its initial length, reoriented, and stretched again. During the motion, the ends of the slender drop become bulbous; figure 5(*k*) (arrow k1) shows that these bulbous ends are about to pinch off from the nearly cylindrical midsection (this is similar to the end-pinching studies of Stone & Leal 1989*a*, *b*). The remaining cylindrical piece, as well as other pieces of fluid cylinders in figure 5 (*k*) (arrows k2 and k3) undergo a similar stretching and folding process.

Other large new drops are the result of breakup of a relatively fat filament, the

pinch-off of a bulbous end or tip of a fold (one can observe many such droplets in figure 5*k*). These new drops might stretch further and develop droplets with two bulbous ends (e.g. arrow l1, figure 5*l*, $t = 300$ s); this mechanism is referred to as necking (Rumscheidt & Mason 1961). In turn, these droplets give birth to two drops with a string of satellite droplets in between. This mode of breakup, which becomes important after 2 periods or so, continues until no more droplets can be stretched and broken anywhere in the flow. When the breakups stop, say after about 10–15 periods ($t = 1500$–2250 s), we say that the drop size distribution has finally reached its equilibrium distribution. The analysis of such a distribution is reserved until §§4.3 and 4.4.

It is rather remarkable that in spite of all of these small-scale processes the motion of the centre of mass of the droplets is almost completely dictated by the macroscopic flow. A clear indication of this fact is provided by a comparison between figures 5(*f*) and 5(*l*). The large U-fold g2 is clearly seen in l2; even though several stretchings and foldings have occurred, the nesting of the broken striations is unmistakable. This type of nesting is characteristic of passive tracers in two-dimensional chaotic flows (Leong & Ottino 1989).

4.2. *Comparison with numerical studies*

In this section, we attempt to develop computational methods which provide some prediction of the experimental results. Ideally we would like to be able to solve an initial-value problem: predict how and when a large fluid drop in a chaotic flow will stretch, deform, and break, and if it does indeed break, to compute the size of the resulting drop fragments. However, such analysis involves tracking of thousands of deformable droplets and their hydrodynamic interactions and, by today's state-of-the-art computing standards, as well as by a comparison with rather simpler problems such as the evolution of a passive tracer in a chaotic flow (Franjione & Ottino 1987), or the precise computation of end-pinching of an extended drop (Stone & Leal 1989*a*), the situation appears to be rather hopeless. The question is: Can we make simplifying assumptions and still obtain reasonable predictions? The answer appears to be yes.

The key assumption is to treat the motion of the centre of mass of the filament as if it were passive. In the beginning of the simulation, we pick the location of the initial condition – a blob consisting of hundreds of points – to match that of the experiment. Then we restart the motion and let the points be convected by the flow. Even though this is a gross approximation, the agreement after the drop is considerably extended is rather good (in experiment 1 this point is reached in about 10–20 s). The next step is to assign a radius to the computed filament corresponding to the experiment itself (using an image analyser). Based on the locations of the previously computed points, we make up a set of new points $\boldsymbol{X}_i$ which constitute a line that goes through the centre mass of the filament (from now on we will refer to the ends of the filament as X_1 and X_2). Each piece of the filament is assigned a (mean) radius, $a_{\mathrm{m}_i} = a_{\mathrm{m}}(\boldsymbol{X}_i)$, and an initial orientation, $\boldsymbol{m}_i = \boldsymbol{m}(\boldsymbol{X}_i)$ proportional to the distance $|\boldsymbol{X}_{i+1} - \boldsymbol{X}_i|$. This creates an array of numbers, a_{m_i} and $\boldsymbol{m}_i$, representing the starting conditions for every segment. The radius and orientation of the ith segment evolves as

$$\dot{a}_{\mathrm{m}_i}/a_{\mathrm{m}_i} = -\tfrac{1}{2}\boldsymbol{D}:\boldsymbol{m}_i\boldsymbol{m}_i, \tag{20}$$

$$\dot{\boldsymbol{m}}_i = \boldsymbol{L}\cdot\boldsymbol{m}_i - (\boldsymbol{D}:\boldsymbol{m}_i\boldsymbol{m}_i)\,\boldsymbol{m}_i. \tag{21}$$

In a chaotic flow the distance $\mathrm{d}s_i = |\boldsymbol{x}_{i+1} - \boldsymbol{x}_i|$ increases exponentially and folds occur.

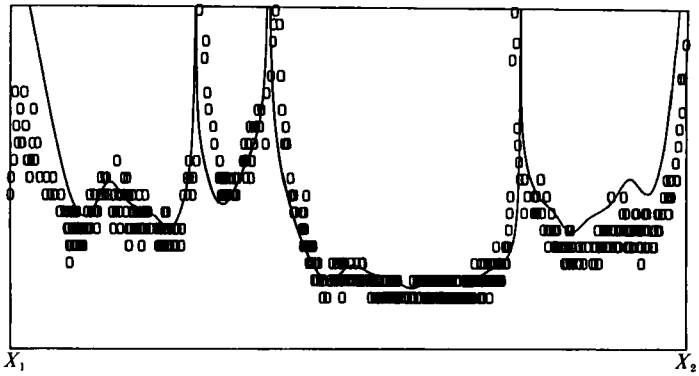

FIGURE 7. Radii of the droplets in figure 6(*e*) versus the computed filament thickness as we unfold the string of droplets and the filament from X_1 to X_2 (X_1 and X_2 are shown in figure 6*e*). Each droplet is represented by the symbol 0; the simulation is represented by the solid line.

In order to capture folds and variation of the radius along the filament, a fluid segment which has stretched such that $\mathrm{d}a_i/\mathrm{d}s_i > \epsilon$ (where ϵ is a small number, we pick $\epsilon = 0.01$) is resegmented and a new radius is obtained by linear interpolation. We use the *ad hoc* model presented in §2 to determine the stability of the fluid segments provided that they are not located near the ends or folds, where the model breaks down. Then the radius of a fluid segment, $a_{\mathrm{m}_i} = a_{\mathrm{m}}(X_i, t)$ is compared with the critical radius, $a_{\mathrm{c}_i} = a_{\mathrm{c}}(X_i, t)$, at every time increment.

How do these predictions compare with the experimental results? There are several ways to test the agreement. A direct comparison between the radius profile of a fluid filament while it is being convected by the flow with the numerical predictions is one possibility. Another possibility is to stop the motion, let the unperturbed filament break, and measure the sizes of the generated drops. Figure 6(*c–e*) (plate 2) shows an experiment with $p = 0.40$. Everything else, including the bulk fluid, is the same as in experiment 1 ($p = 0.067$). Figure 6(*c*), which looks very similar to figure 5(*f*), is taken immediately after the flow is stopped, $t = 150$ s. The only qualitative difference between the two photographs is that figure 6(*c*) does not show any visible sign of capillary disturbances, whereas in figure 5(*f*) there are some instabilities developed near the U-fold. This is not surprising since the characteristic velocity for the interfacial-tension-driven changes is given by $u_\sigma = \sigma/\mu_{\mathrm{e}}(1+p)$; hence the instability growth on the filament with higher viscosity ratio is delayed.

After the flow stops, figure 6(*c*), breakup occurs starting primarily in the thinner parts of the filament ($O(10)$ s). Then, as expected, it slowly propagates to the thicker regions of the filament ($O(100)$ s) (figure 6*d*). Figure 6(*e*) shows the result after all fluid filaments are broken. The sizes of the drops as well as their distances from one another are measured with the aid of a stereomicroscope and the distances along the length of the filament recorded (in carrying out these measurements we do not count the satellite drops but use them only as reference points).

Figure 6(*f*) shows the corresponding computer-generated picture of the unbroken fluid filament. The thickness of the filament, which is shown to scale, is related to the amount of length stretch, which is shown according to a colour scale. Notice that U- and V-folds have been subjected to much less stretching than other parts of the filament. Other computations seem to indicate that this is rather common. In general the agreement between the results of figure 6(*c,f*) is good. Figure 7 shows the radii of the droplets – each represented by the symbol 0 – and rescaled according to

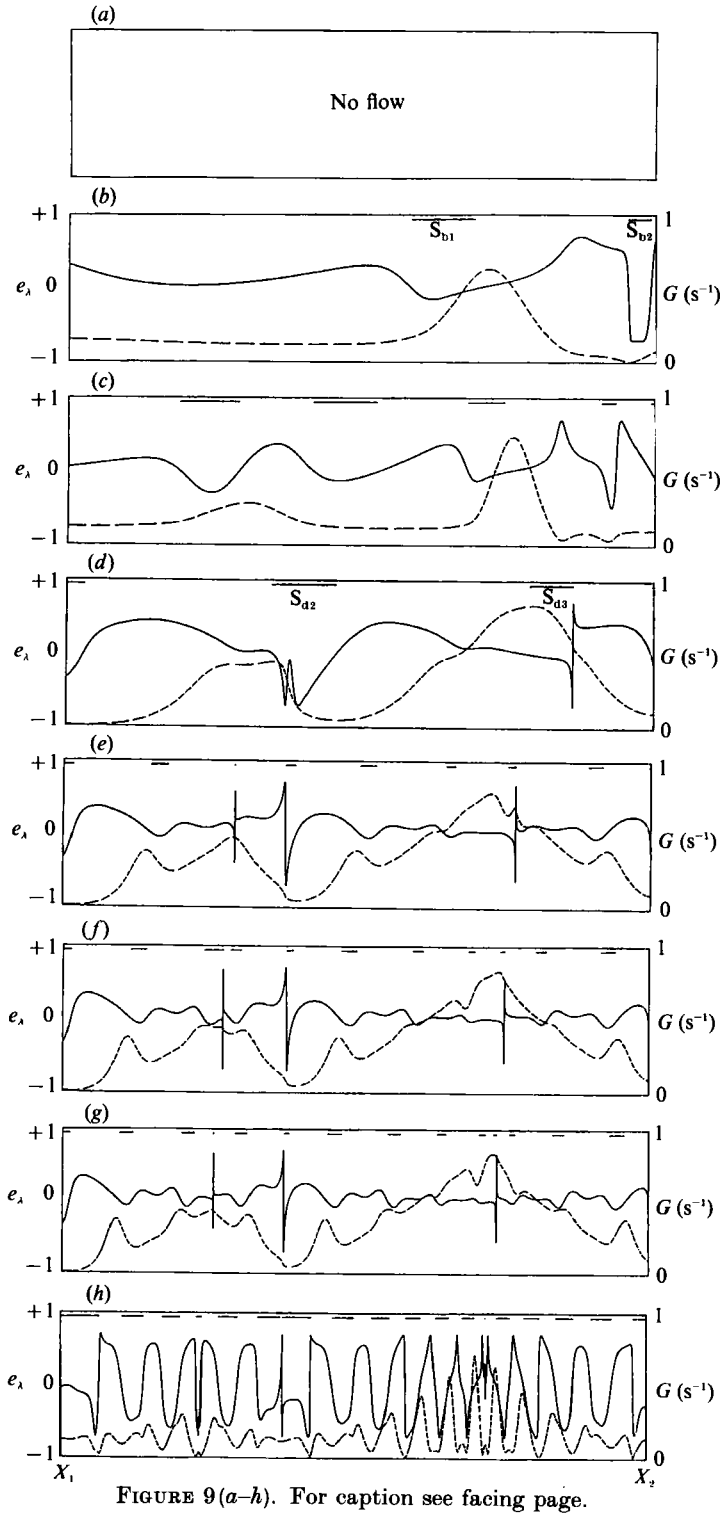

FIGURE 9(*a–h*). For caption see facing page.

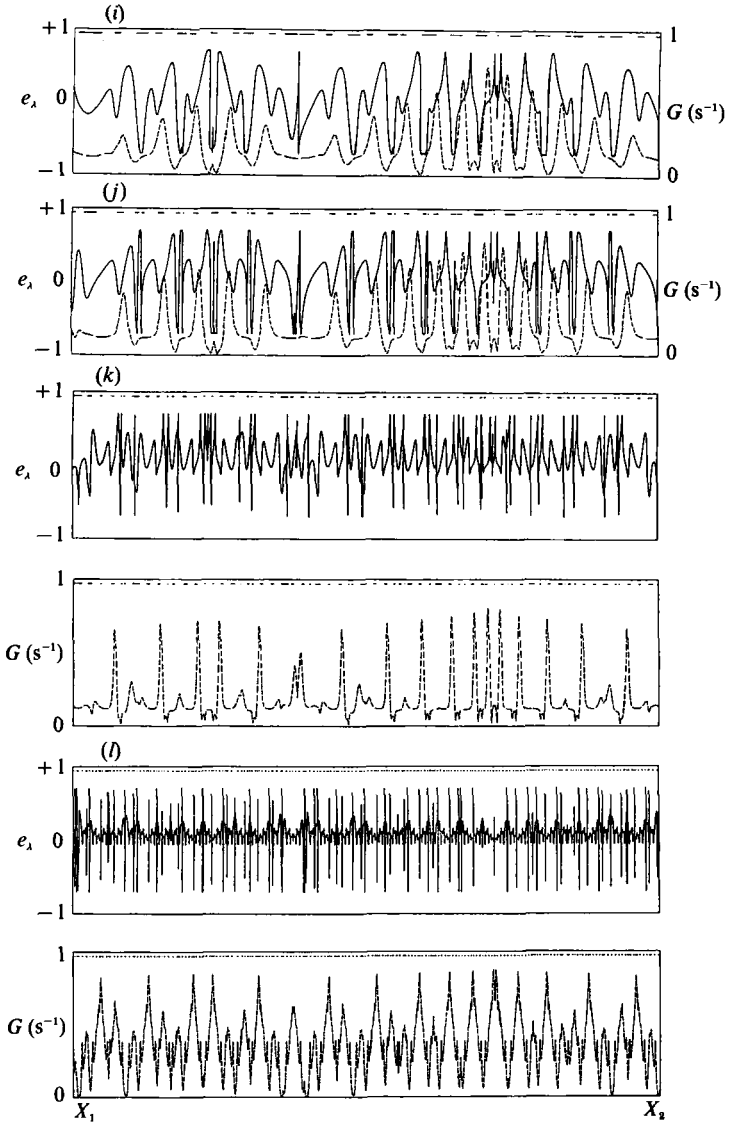

FIGURE 9. Kinematical histories along the filament corresponding to experiment 1. The first frame (*a*), purposely left blank, corresponds to the initial condition. (*b–l*) Values of both e_λ (solid line) and G (dashed line) are shown. The discontinuous solid lines parallel to the x-axis correspond to the locations where the stretching is negative.

equation (14) – versus the computed filament thickness, represented by the solid line. There is total of 1111 mother drops. With a few exceptions, the agreement is satisfactory.

It is apparent that we are able to follow a fluid segment and keep a fairly accurate track of the evolution of its radius provided that: (i) it is not located near the ends of the filament, and (ii) it is not near the folds. Figure 8(*a–l*) (plate 3) shows patterns produced by the stretched and folded filaments tailored to mimic the experiments of figure 5(*a–l*). The filament is coloured according to the stretching experienced by different parts of it: red when the stretching is positive, blue when it is negative. The quantitative companions of these photographs, which show the values of both e_λ and

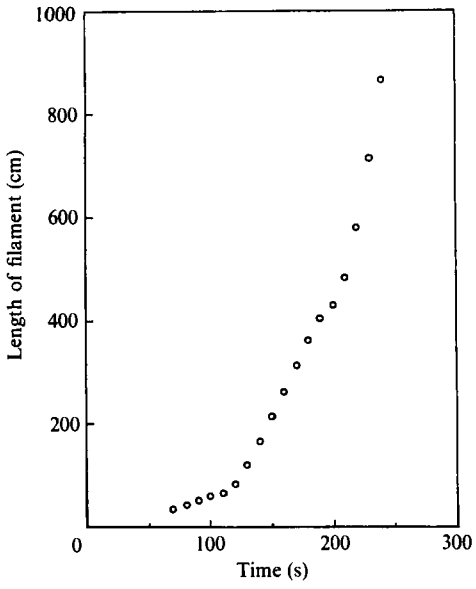

FIGURE 10. Length of the filament as a function of time corresponding to the computation shown in figure 8 (compare with experiments in figure 5).

G as we unfold the filament from X_1 to X_2, are shown in figure 9(*a–l*). Figure 10 shows the length of the filament from X_1 to X_2 as a function of time corresponding up to figure 8(*l*); the length stretch is approximately 2×10^3. Experiments, figure 5, show that the filament can be stretched approximately a thousand times before breakup becomes apparent (figure 5*g*).

The matching between the orientations of the unbroken liquid threads (figure 5*a–f*) with the simulation (figure 8*a–f*) is good and confirms that the drop stretches as a material line. Most of the small droplet fragments which result after the breakups (figure 5*g–k*) can be superimposed reasonably well on top of the computer-generated patterns shown in figure 8(*g–k*). Some of the larger droplets, however, 'stray off course' (see figure 5*l*). Our experimental observations suggest that this is related to asymmetries in the drop shapes. A periodic restoration to symmetry or a combination of asymmetric deformations results in a migration of the centre of mass of the drop. A small deviation, given the fact that the flows are chaotic, results in a large displacement with respect to well-behaved former neighbours.

For the first few photographs (figure 8*a–f*), it is possible to trace the filament along its length and identify the values of e_λ and G shown in figure 9(*a–f*). Figure 9(*a*) is purposely left blank to match the initial condition ($t = 0$ s, no deformation). In general, the filament experiences a complex variation of stretching and compression along its length. For example, figure 9(*b*) shows that there are two segments, denoted S_{b1} and S_{b2}, where the fluid thread is compressed ($e_\lambda < 0$). These changes of stretching sign are important. The rate of change of stretching along the filament, $\mathrm{d}e_\lambda/\mathrm{d}s$, varies depending on the orientation of the filament with respect to the local flow $\boldsymbol{L}(\boldsymbol{X}, t)$. Since $\boldsymbol{L}$ is approximately uniform near the tip of the fold, it is apparent that as the filament adopts all possible positions with respect to the eigenvalues of $\boldsymbol{L}$, $\mathrm{d}e_\lambda/\mathrm{d}s$ changes sign. Thus, folds are associated with a stretching–compression transition. This is confirmed by an examination of figure 8. In fact, an examination of the e_λ profiles gives a good indication of whether or not a filament is folded. Let us examine this point more closely.

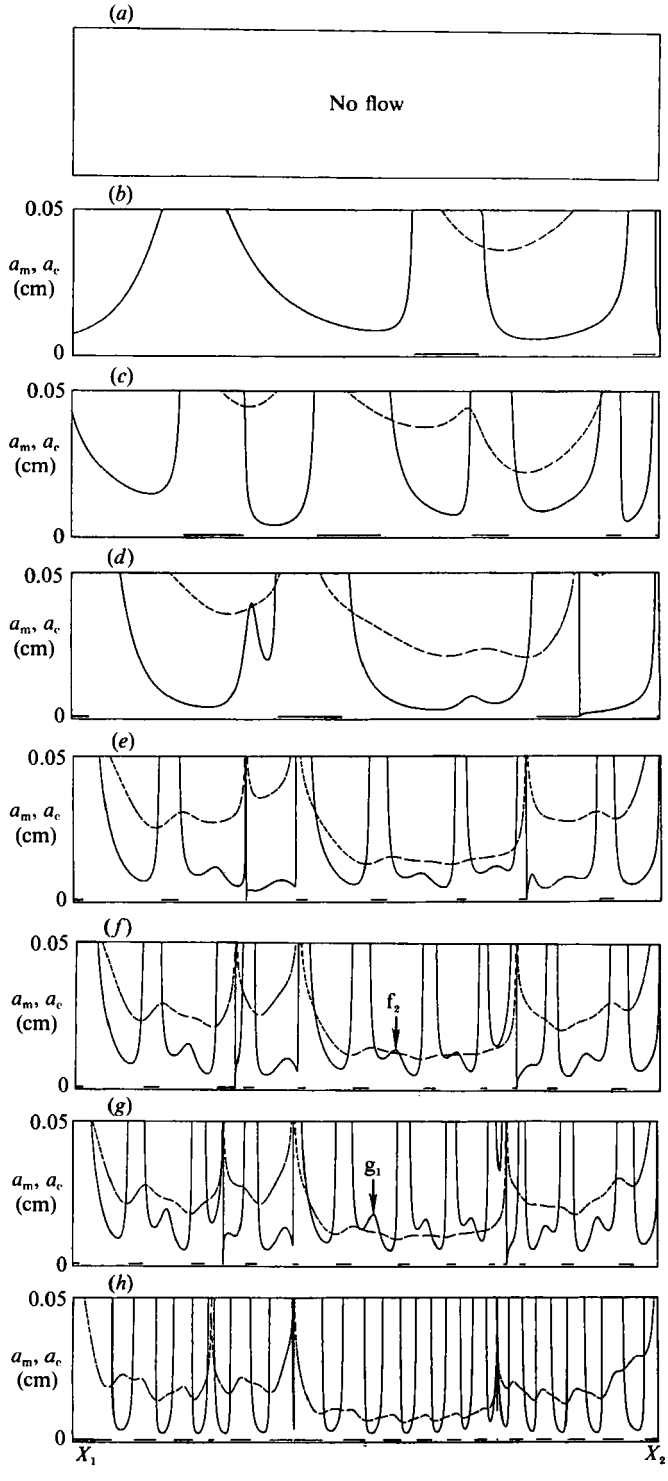

FIGURE 11. Mean radius of the filament, a_m (dashed line), along with its critical radius, a_c (solid line). The comparison is valid as long as $e_\lambda > 0$ (the discontinuous solid lines parallel to the x-axis correspond to the locations where the stretching is negative). Notice that the arrows shown correspond to the ones shown in figure 5.

Figure 8(*d*) shows the pattern when the inner wall has just started to move clockwise and the filament is adjusting its orientation to the new flow. The companion stretching profile in figure 9(*d*) shows that near S_{d2}, the stretching e_λ has a local maximum and two minima, indicating that two new folds are about to be formed. A more pronounced spike is shown in S_{d3} suggesting extreme curvature; an examination of figure 8(*d*) shows that this piece turns out to be a V-fold. (Note that the increase in curvature is due, in part, to the rescaling of the length of the filament. Other ways of displaying these results though, do not seem to be as convenient.) Figure 9(*e–g*) shows that S_{d2} evolves into two folds, a V-fold and a U-fold, as seen earlier in experiment 1 (figure 5*e–g*). Subsequently, when the filaments have been elongated by more periods of the flow, the stretching profiles look rather complicated (figure 9*h–l*). However, a closer examination of figure 9(*k* or *l*), reveals that the variation of e_λ and G along the filament consists of identifiable repeating units. The reason for this behaviour is that neighbouring nested filaments experience nearly identical flow histories.

The information contained in figures 8(*a–l*) and 9(*a–l*) provides explanations for many of the results seen in experiment 1. For example, figure 5(*f*) shows that a relatively thick fluid thread fractures unexpectedly at a point marked by arrow f1. Figure 8(*f*) indicates that the instability is growing precisely at a location where e_λ is negative, i.e. the filament is being compressed. Furthermore, an examination of the history experienced by this particular segment reveals that the filament has experienced relatively low values of shear rates (figure 9*d–f*). Therefore, the flow near the filament has not contributed much in damping the disturbances and, in fact, we can envision that the fluid near the fold is nearly stagnant. The characteristic velocity for the interfacial-tension-driven changes, given by $u_\sigma = \sigma/\mu_e(1+p)$, is larger than the characteristic velocity of the flow, denoted by $u_G = Gl_c$ (l_c is some characteristic lengthscale of the apparatus). As a result, the interfacial-tension-driven motion magnifies the instabilities and breakup occurs.

Figure 11(*a–h*) shows the time evolution of the mean radius of the filament in experiment 1, denoted a_m (dashed line), along with its corresponding critical radius, a_c (solid line), computed as indicated in §2. The discontinuous solid lines parallel to the x-axis indicate the locations where e_λ is negative (compression). Figure 11(*a–h*) shows that the radius a_m is continuously decreasing whereas the critical radius a_c fluctuates depending on the local values of e_λ and G. It is possible that during the flow the radius a_m is less than a_c for a short period of time; in such a case any instabilities which manage to grow might be damped again. Eventually the radius a_m might be less than a_c for a sufficient time to cause breakup.

The computational results are consistent with experiment 1. No capillary instabilities are observed along the filaments before $t = 150$ s. At $t = 150$ s (figure 5*f*), a magnification at arrow f2, shows that some instabilities are starting to grow (see figure 11*f*). A few breakups occur a few seconds later, and since the radius a_m is still less than a_c (figure 11*g*), breakups continue to occur (see figure 5*g*, $t = 160$ s). The exact locations of the breakups, predicted from the simulation, are shown in figure 12(*a–c*) (plate 4). The regions where $a_m < a_c$ are marked in yellow. The comparison between computation and experiment is good only for the first few breakups; subsequently the end effects of the many pieces of the broken filaments become increasingly important and the agreement is lost.

4.3. *Effects of viscosity ratio*

The results presented in this section correspond to the flow of experiment 1; the initial conditions are identical as well. The objective of the experiments is to investigate the effect of viscosity ratio on modes of breakup. The main results are shown in figure 13 and correspond to four different experiments – denoted A, B, C, and D – with viscosity ratios $p = 0.010$, 0.067, 0.40, and 2.8 respectively. The superscript following the designation A, B, C, D, corresponds to the end of the period in which the picture was taken. Equilibrium drop size distributions, obtained via image analysis, are shown in figure 14.

The most important observations are the following. Low-viscosity-ratio drops stretch more passively but extend relatively little, $O(10^1–10^2)$, before they break producing large droplets. These large droplets may undergo subsequent stretching, folding, and breakup. Under identical conditions, high-viscosity-ratio drops stretch substantially, $O(10^2–10^4)$, before the break producing very small fragments; these small fragments rarely break again. On the average, we find that the mean drop size decreases with increasing p. The equilibrium size distributions corresponding to high-viscosity-ratio drops are more non-uniform than those corresponding to low viscosity ratios. This is primarily due to the existence of rather large droplets produced via fold-pinching or end-pinching, which resist further breakup.

Some of these results can be rationalized in terms of characteristic times: roughly speaking the characteristic time of the flow is $t_G = 1/G$ whereas the characteristic time of the interfacial-driven motion is given by $t_\sigma = \zeta\mu_e(1+p)/\sigma$, where ζ is some characteristic lengthscale (for a drop, $\zeta = r_d$, for a filament, $\zeta = a_m$). In general, when the flow stops, or when G is very small, the motion of the drop/filament motion is driven strictly by interfacial tension. But when G is finite the shear response can be significant enough to counter interfacial tension forces. The ratio $t_\sigma/(1+p)\,t_G$ is the capillary number (the factor $(1+p)$ is added to be consistent with the definition of the capillary number given by Bentley & Leal 1986 and others). In our case we have access to both G and ζ_c (i.e. the critical radius of a drop or a filament) from the simplified model of §§ 2 and 4.2. Therefore we can compare the ratio $t_\sigma/(1+p)\,t_G$ with a critical capillary number in order to determine whether a drop/filament is going to extend or break. For a droplet in a quasi-steady flow this piece of information is already available. Bentley & Leal (1986) obtained experimentally the critical capillary number, $Ca_{d,c}$, as a function of the viscosity ratio p and flow type K. Similarly, in the case of an *extending filament* we can use the results from § 2 to obtain the critical capillary number, $Ca_{f,c}$, as a function of stretching rate α_λ, shear rate G, interfacial tension, σ, and viscosity ratio p. Naturally, in a complex flow such as ours, the parameters K, α_λ, and G change in time in a rather complicated fashion (see figure 4). Nevertheless we can still make useful estimates at particular instants of time by comparing the ratio $t_\sigma/(1+p)\,t_G$ with the critical capillary numbers $Ca_{d,c}$ or $Ca_{f,c}$. Some of these estimates are made below to interpret the experimental results.

Let us now consider experiments A–D in terms of results obtained for linear flows. The size of the initial drops in experiments A–D is fairly large and $t_\sigma/(1+p)\,t_G$ is about 7.5. Bentley & Leal show that for K between 0 and 1, and for p between 0.01 to about 3, $Ca_{d,c}$ ranges from 0.1 to 0.5 (see figure 28 of their 1986 paper). Consequently the initial drops extend into filaments. After extension, the drops in the low-viscosity-ratio system ($p < 1$) behave nearly passively. Note, for example, that figure 13 (A^1–C^1) can be superimposed reasonably well on top of the computer-generated patterns of figure 8(f). On the other hand, high-viscosity-ratio ($p > 1$) filaments (for

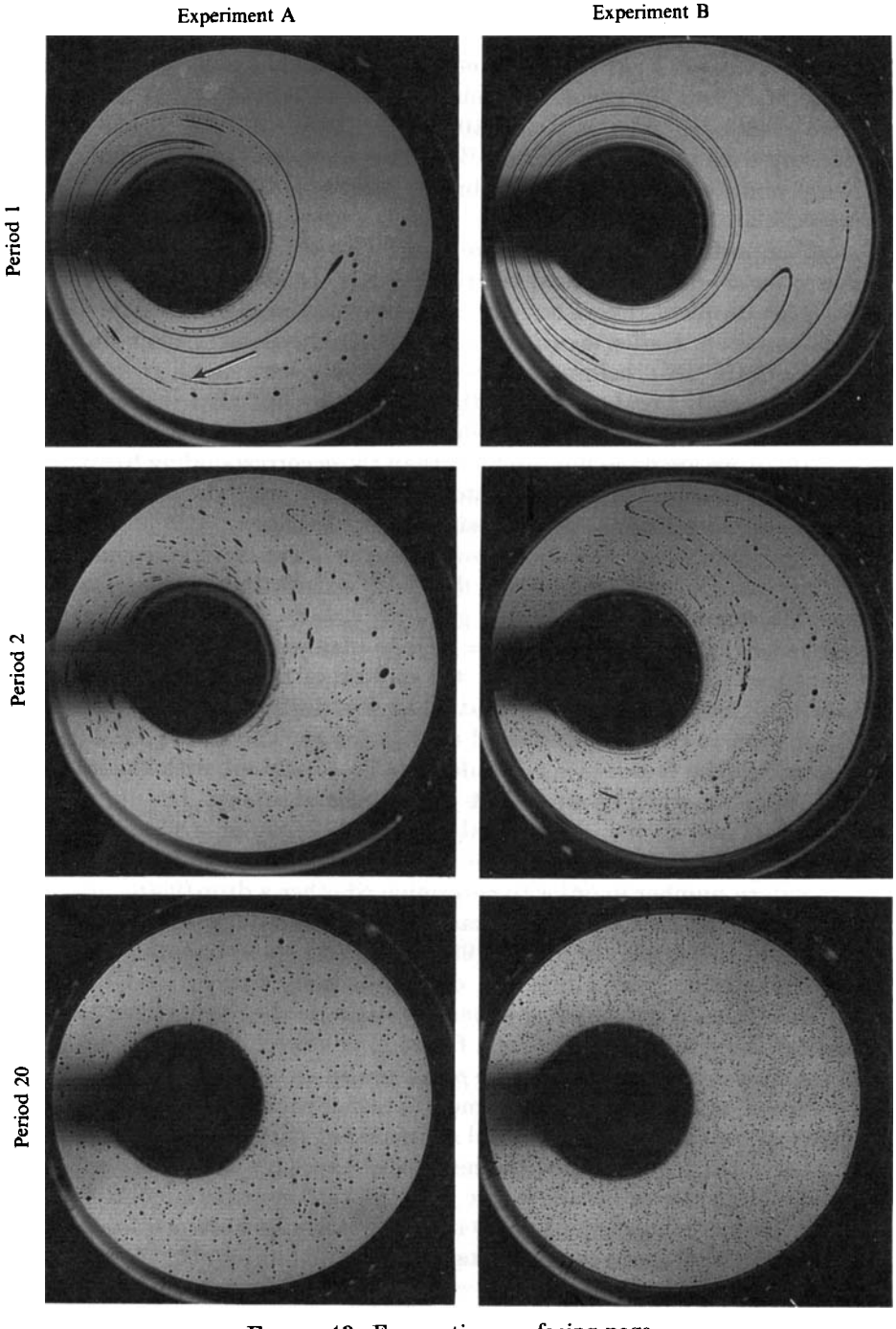

FIGURE 13. For caption see facing page.

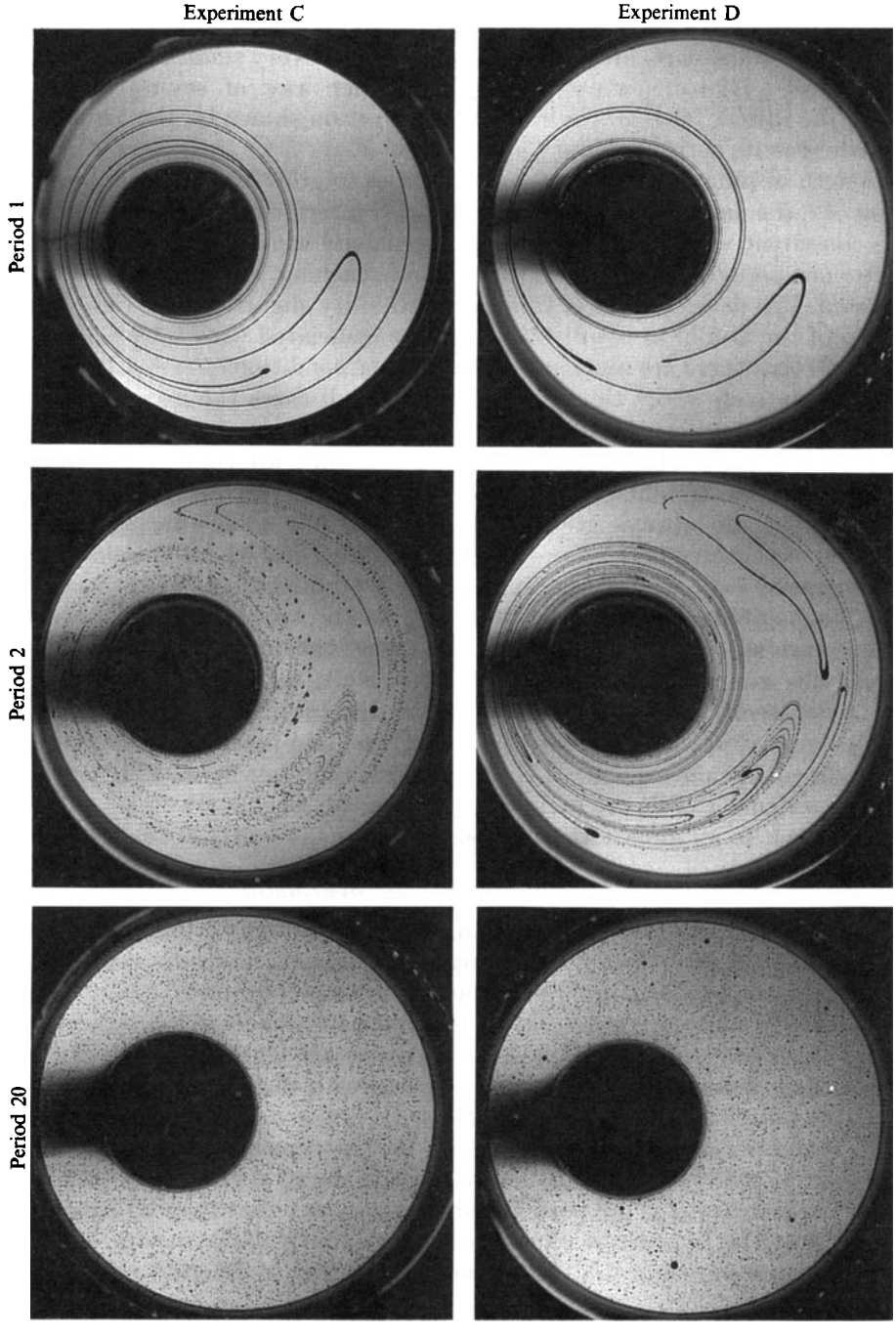

FIGURE 13. Effect of viscosity ratio on modes of breakup. Experiment A corresponds to $p = 0.010$, B to 0.067, C to 0.40, and D to 2.8.

example see experiment D) show some noticeable deviations with respect to the passive case. Note as well that the amount of time needed to elongate a spherical drop is a strong function of t_σ. The most viscous drop (experiment D) requires roughly three times as long in order to achieve the same length as its less viscous

counterparts (experiments B, C). Figure 13(A^1) shows that in the low-viscosity-ratio case ($p = 0.010$) significant breakup occurs during the flow. Figure 9(*b–e*) shows that during the flow some parts of the filament experience a very small G, hence satisfying the condition $t_\sigma/(1+p)\,t_G < Ca_{t,c}$ (this is another way of saying $a_m < a_c$); for example, the ratio $t_\sigma/(1+p)\,t_G$ is 0.076 at the position shown by the arrow in figure 13(A^1) whereas its corresponding $Ca_{t,c}$ is 0.15.

The length of time required by the instabilities to grow and result in breakup is a function of t_σ (i.e. large t_σ results in more sluggish interfacial-tension-driven motion). This is consistent with our results; the experiments with larger t_σ – B, C, D – show that after one period, with the exception of end-pinching, the filaments have not yet fragmented. The development of capillary instability slightly to the right-hand side of the tip of the U-fold in figure 13(B^1) can be associated with $t_\sigma/(1+p)\,t_G < Ca_{t,c}$. Note as well that there are segments satisfying the condition $t_\sigma/(1+p)\,t_G < Ca_{t,c}$ but only for a relatively short time (i.e. $t < t_\sigma$). In such cases the instabilities are not given enough time to cause breakup before they are damped again.

On the other hand instabilities grow when filaments are compressed. Since folds are associated with stretching–compression transitions every fold has a region where the instabilities are always growing. Breakup at the folds (during the flow) is observed in experiment 1 (see for example arrows g2 and h1 in figure 5), as well as the low-viscosity-ratio experiment in figure 13(A^1) (notice that a great part of the U-fold has fragmented, also the tip of the V-fold has broken as well). The instabilities at the folds are not visible in figure 13(C^1, D^1) since the disturbances are damped by increasing the viscosity of either phase. As a result, high-viscosity-ratio filaments stretch a lot more before breaking resulting in tiny fragments. However, the relatively large droplets which are produced via fold-pinching and end-pinching rarely undergo any subsequent stretching and breakup (see figure 13D^2); these large droplets (see figure 13D^{20}) are periodically extended, when $t_\sigma/(1+p)\,t_G > Ca_{d,c}$, but they relax back to an almost spherical shape when $t_\sigma(1+p)\,t_G < Ca_{d,c}$.

4.4. *Analyses of drop size distribution*

In order to quantify the equilibrium drop size distribution we took photographs of the experiments described in §4.3, enlarged the images, then divided them up in 50–60 subsections, and digitized the pictures. Very small droplets, possibly satellites or sub-satellites, which are not visible through the camera lense are neglected in the analyses. However, even when the smallest drops are ignored, the measured drop sizes span four decades in volume. This generates a distribution $f(V, p)$, where V denotes the volume of the drops and $f(V, p)\,\mathrm{d}V$ is the number of drops with sizes between V and $V+\mathrm{d}V$. Figure 14(*a*) shows the distributions corresponding to the experiments of figure 13 after 20 periods. Each curve corresponds to 1500–2000 droplets; the distributions are normalized in such a way that they all have the same number of droplets. In order to verify the reproducibility of the results several of the runs experiments were repeated. Results corresponding to different repetitions were virtually identical.

The curves corresponding to $p = 0.010$, 0.067, and 0.40, have similar shapes. On the other hand, as might have been expected based on the discussion at the end of §4.3, the curve corresponding to $p = 2.8$ has a different shape. At equilibrium, the sizes of the large drops fall inside an envelope indicated by the dashed line. Any drop on the right-hand side of the envelope will break again. The plot shows that at equilibrium the number of small drops is much greater than the number of large droplets, and as expected, within the range of viscosity ratio studied, the size of these

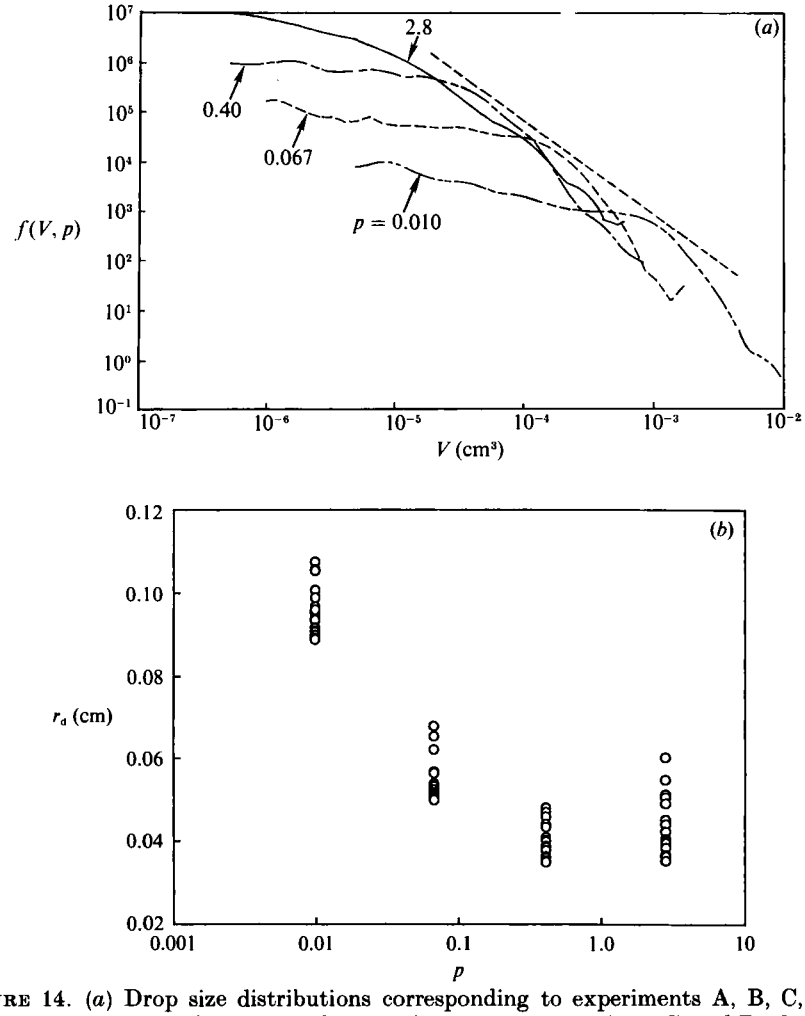

FIGURE 14. (*a*) Drop size distributions corresponding to experiments A, B, C, and D after 20 periods. (*b*) The radii of 20 largest droplets from experiments A, B, C, and D after 20 periods as a function of the viscosity ratio p.

smaller droplets decreases as the viscosity ratio increases. However, this trend does not apply to the larger droplets. Figure 14(*b*) shows the radii of the 20 largest droplets from each experiment as a function of their viscosity ratio. The plot suggests a minima between $p = 0.40$ and $p = 2.8$.

The repetitive nature of chaotic mixing, stretching and folding, as well as the repetitive nature of the breakup process itself, suggest that the equilibrium drop size distribution might, in some sense, be self-similar, i.e. there might be a way to collapse all distributions into a single curve. In order to check this point we use scaling techniques similar to those employed in critical phenomena (Hohenberg & Halperin 1977), aggregation theory (Meakin 1988 and references therein), and diffusion-reaction dynamics (Muzzio & Ottino 1989). The basic idea is to rescale the distribution $f(V, p)$ into a distribution of the form

$$\mathscr{F}(y) = V^{\theta} f(V, p), \tag{22}$$

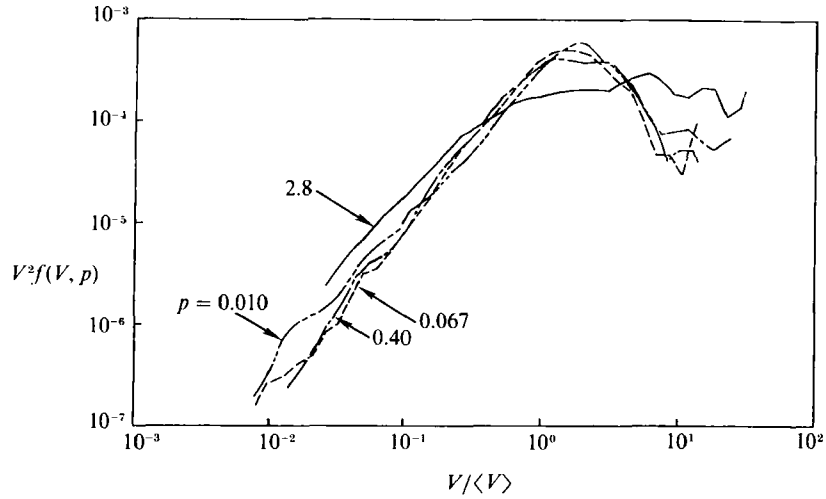

FIGURE 15. Rescaled drop size distributions for four different viscosity ratios ($p = 0.010$, 0.067, 0.40 and 2.8). The data correspond to experiments A, B, C, and D after 20 periods.

where $y = V/\langle V\rangle$, $\langle V\rangle$ is the arithmetic mean of volume sizes V, and θ is some exponent to be determined. If scaling exists, $\mathscr{F}(y)$ is the same for all distributions. The first moment of all the distributions, M_1, is given by,

$$M_1 = \int_0^\infty Vf(V,p)\,\mathrm{d}V = \int_0^\infty V^{1-\theta}\mathscr{F}(y)\,\mathrm{d}V = \langle V\rangle^{2-\theta}\int_0^\infty y^{1-\theta}\mathscr{F}(y)\,\mathrm{d}y. \tag{23}$$

Since by normalization, M_1 (total number of drops) is constant, and since by assumption, $\mathscr{F}(y)$ is independent of p, then $\theta = 2$. A rescaling of the form $V^2f(V,p)$ *vs.* $V/\langle V\rangle$ shows that this expectation is confirmed (see figure 15); all curves collapse into a master curve except for the case corresponding to the largest viscosity ratio ($p = 2.8$). The success of scaling might be attributed in part to the underlying scaling structure of the stretching process itself (Muzzio, Swanson & Ottino 1991) and the deviation of the case $p > 1$ to the different nature of the breakup mechanism. In fact, more extensive studies suggest that there are two scaling families and that the same results are present even in partially chaotic flows (Muzzio, Tjahjadi & Ottino 1991).

5. Conclusions

A drop of an immiscible fluid placed in a chaotic flow is subjected to a deformation history including both stretching and compression. These actions lead to breakup and dispersion. In this work we have presented experimental results and tried to rationalize the results by means of computations. The experimental results are representative of a large number of repeated experiments and we have tried to focus on the most important phenomena. We have observed that breakup in chaotic flows presents some interesting qualitative differences compared to breakup in linear flows. However, some of the results obtained in terms of linear flows, especially those spanning a range between shear and elongation (e.g. Bentley & Leal 1986), provide considerable guidance in the interpretation of the results.

Within chaotic regions, on the average, the net stretching is positive and when the viscous force is strong enough to overcome the interfacial tension the drop deforms and forms a long fluid thread increasing its length exponentially. However,

behaviour can be heavily dependent upon the initial placement of the blob. For example, droplets placed within regular islands might not break at all whereas chaotic regions produce thousands of drops (an example of this phenomenon appears in figure 2 of Ottino 1990). Therefore, in order to apply these results to chaotic flows it is first necessary to identify the locations and motions of the regular islands. This can be accomplished by means of computations or by careful experimentation (Leong & Ottino 1989).

Chaotic flows typically fold fluid filaments and produce rather large variations of stretching and compression along the threads. This produces some modes of breakup that cannot happen in linear flows. The primary example is breakup in folds which is associated with a change of sign in stretching rate. A sufficiently extended filament that finds itself in a region of compression is susceptible to breakup. However, the primary mode of breakup during the initial stages of the process is capillary wave instabilities; other modes of breakup such as necking, end-pinching, and fold-pinching occur as well.

An *ad hoc* model assuming that moderately extended filaments behave passively is an excellent approximation especially for drops with low viscosity ratio ($p < 1$). In our experiments low-viscosity-ratio drops stretch passively but extend relatively little, $O(10^1$–$10^2)$, before they break, resulting in the formation of large droplets. These large droplets may undergo subsequent stretching, folding, and breakup. Under identical conditions, droplets in systems with $p > 1$ stretch substantially, $O(10^2$–$10^4)$, before they break, producing very small fragments; these small fragments rarely break again. The equilibrium size distributions corresponding to $p > 1$ are more non-uniform than those corresponding to low viscosity ratios, but in general the mean drop size decreases as the viscosity ratio increases. This is primarily due to the existence of rather large droplets produced via fold-pinching and/or end-pinching, which resist further breakup.

Our simplified analysis is applicable to fully extended filaments with negligible bending. In order to zoom into the details of breakup of a folded filament, or the formation of the satellites, sub-satellites, etc., it appears necessary to resort to more sophisticated numerical techniques, such as the boundary-integral methods (Rallison & Acrivos 1978; Stone & Leal 1989*a*, *b*; Mansour & Lundgren 1990). One of the things that should be investigated in this regard is the scaling in satellite size with the viscosity ratio. This scaling might be related to the results obtained regarding the scaling drop size distribution corresponding to different viscosity ratios.

In this study we have presented experimental results that illustrate phenomena that occur when filaments are stretched and folded – by several orders of magnitude – in chaotic flows. In principle, these results or suitable experimental and computational extensions, should allow the design of fluid motions capable of achieving pre-established breakup conditions. Such a study will require knowing more about the typical flow histories experienced by fluid elements in typical chaotic flows (Muzzio, Swanson & Ottino 1990). Nevertheless, it appears that further studies of breakup in chaotic flows should be relevant to the design of mixing devices and to the understanding of processes involving flows of immiscible fluids.

This work was supported by the Department of Energy, Office of Basic Energy Sciences. We would like to thank Fernando J. Muzzio for his assistance with the results of §4.4 and Paul D. Swanson for his critical reading of the manuscript.

REFERENCES

Acrivos, A. 1983 The breakup of small drops and bubbles in shear flows. *Ann. NY Acad. Sci.* **404**, 1–11.

Aref, H. & Balachandar, S. 1986 Chaotic advection in a Stokes flow. *Phys. Fluids* **29**, 3515–3521.

Bentley, B. J. & Leal, L. G. 1986 An experimental investigation of drop deformation and breakup in steady two-dimensional linear flows. *J. Fluid Mech.* **167**, 241–283.

Chaiken, J., Chevray, R., Tabor, M. & Tan, Q. M. 1986 Experimental study of Lagrangian turbulence in a stokes flows. *Proc. R. Soc. Lond.* A **408**, 165–174.

Franjione, J. G. & Ottino, J. M. 1987 Feasibility of numerical tracking of material lines and surfaces in chaotic flows. *Phys. Fluids* **30**, 3641–3643.

Grace, H. P. 1971 Dispersion phenomena in high viscosity immiscible fluid systems and application of static mixers as dispersion devices in such systems. *3rd Engng Found. Res. Conf. Mixing, Andover, NH.* (Published in *Chem. Engng Commun.* **14** (1982), 225–277.)

Hohenberg, P. C. & Halperin, B. I. 1977 Theory of dynamical critical phenomena. *Rev. Mod. Phys.* **49**, 435–479.

Khakhar, D. V. & Ottino, J. M. 1987 Breakup of cylindrical fluid threads in linear flows. *Intl J. Multiphase Flow* **13**, 71–86.

Kuhn, W. 1953 Spontane Aufteilung von Flüssigkeitszylindern in kleine Kugeln. *Kolloid Z.* **132**, 84–99.

Lee, W. K. & Flumerfelt, R. W. 1981 Instability of stationary and uniformly moving cylindrical fluid bodies – I. Newtonian systems. *Intl J. Multiphase Flow* **7**, 363–384.

Leong, C. W. & Ottino, J. M. 1989 Experiments on mixing due to chaotic advection in a cavity. *J. Fluid Mech.* **209**, 463–499.

Mansour, N. N. & Lundgren, T. S. 1990 Satellite formation in capillary jet breakup. *Phys. Fluids* A **2**, 1141–1144.

Meakin, P. 1988 Fractal aggregates and their fractal measures. In *Phase Transitions and Critical Phenomena* (ed. C. Domb & J. L. Lebowitz), vol. 12, pp. 335–489. Academic.

Mikami, T., Cox, R. & Mason, R. G. 1975 Breakup of extending liquid threads. *Intl J. Multiphase Flow* **2**, 113–118.

Muzzio, F. J. & Ottino, J. M. 1989 Dynamics of a lamellar system with diffusion and reaction: scaling analysis and global kinetics. *Phys. Rev.* A **40**, 7182–7192.

Muzzio, F. J., Swanson, P. D. & Ottino, J. M. 1991 The statistics of stretching and stirring in chaotic flows. *Phys. Fluids* A **3**, 822–834.

Muzzio, F. J., Tjahjadi, M. & Ottino, J. M. 1991 Self-similar drop size distributions produced by breakup in chaotic flows. *Phys. Rev. Lett.* **67**, 54–57.

Ottino, J. M. 1989 *The Kinematics of Mixing: Stretching, Chaos, and Transport.* Cambridge University Press.

Ottino, J. M. 1990 Mixing, chaotic advection, and turbulence. *Ann. Rev. Fluid Mech.* **22**, 207–253.

Rallison, J. M. 1984 The deformation of small viscous drops and bubbles in shear flows. *Ann. Rev. Fluid Mech.* **16**, 45–66.

Rallison, J. M. & Acrivos, A. 1978 A numerical study of the deformation and burst of a viscous drop in an extensional flow. *J. Fluid Mech.* **89**, 191–209.

Rumscheidt, F. D. & Mason, S. G. 1961 Particle motions in sheared suspensions. XII. Deformation and burst of fluid drops in shear and hyperbolic flow. *J. Colloid Sci.* **16**, 238–261.

Rumscheidt, F. D. & Mason, S. G. 1962 Breakup of stationary liquid threads. *J. Colloid Sci.* **17**, 260–269.

Stone, H. A. & Leal, L. G. 1989*a* Relaxation and breakup of an initially extended drop in an otherwise quiescent fluid. *J. Fluid Mech.* **198**, 399–427.

Stone, H. A. & Leal, L. G. 1989*b* The influence of initial deformation on drop breakup in subcritical time-dependent flows at low Reynolds number. *J. Fluid Mech.* **206**, 223–263.

Swanson, P. D. & Ottino, J. M. 1990 A comparative computational and experimental study of chaotic mixing of viscous fluids. *J. Fluid Mech.* **213**, 227–249.

TAYLOR, G. I. 1934 The formation of emulsions in definable fields of flow. *Proc. R. Soc. Lond.* A **146**, 501–523.

TJAHJADI, M. & OTTINO, J. M. 1990 Breakup and dispersion of highly stretched droplets in a chaotic flow field. *Phys. Fluids* (*Gallery of Fluid Motion*) A **2**, 1524.

TOMOTIKA, S. 1935 On the stability of a cylindrical thread of a viscous liquid surrounded by another viscous fluid. *Proc. R. Soc. Lond.* A **150**, 322–337.

TOMOTIKA, S. 1936 Breaking up of a drop of viscous liquid immersed in another viscous fluid which is extending at a uniform rate. *Proc. R. Soc. Lond.* A **153**, 302–318.

WANNIER, G. H. 1950 A contribution to the hydrodynamics of lubrication. *Q. Appl. Maths* **8**, 1–32.